Stem Cell Reports
Article

OPEN ACCESS

Genomic Analysis Reveals Disruption of Striatal Neuronal Development and Therapeutic Targets in Human Huntington's Disease Neural Stem Cells

Karen L. Ring,[1,3] Mahru C. An,[1,3] Ningzhe Zhang,[1] Robert N. O'Brien,[1] Eliana Marisa Ramos,[2] Fuying Gao,[2] Robert Atwood,[1] Barbara J. Bailus,[1] Simon Melov,[1] Sean D. Mooney,[1] Giovanni Coppola,[2] and Lisa M. Ellerby[1,*]

[1]Buck Institute for Research on Aging, Novato, CA 94945, USA
[2]Departments of Neurology and Psychiatry, Semel Institute for Neuroscience and Human Behavior, David Geffen School of Medicine, University of California, Los Angeles, CA 90095, USA
[3]Co-first author
*Correspondence: lellerby@buckinstitute.org
http://dx.doi.org/10.1016/j.stemcr.2015.11.005

SUMMARY

We utilized induced pluripotent stem cells (iPSCs) derived from Huntington's disease (HD) patients as a human model of HD and determined that the disease phenotypes only manifest in the differentiated neural stem cell (NSC) stage, not in iPSCs. To understand the molecular basis for the CAG repeat expansion-dependent disease phenotypes in NSCs, we performed transcriptomic analysis of HD iPSCs and HD NSCs compared to isogenic controls. Differential gene expression and pathway analysis pointed to transforming growth factor β (TGF-β) and netrin-1 as the top dysregulated pathways. Using data-driven gene coexpression network analysis, we identified seven distinct coexpression modules and focused on two that were correlated with changes in gene expression due to the CAG expansion. Our HD NSC model revealed the dysregulation of genes involved in neuronal development and the formation of the dorsal striatum. The striatal and neuronal networks disrupted could be modulated to correct HD phenotypes and provide therapeutic targets.

INTRODUCTION

Huntington's disease (HD) is a debilitating, inherited neurological disorder characterized by chorea, psychological changes, and cognitive decline leading to dementia (Victorson et al., 2014). These symptoms are correlated with loss of striatal and cortical neurons in the brain (Ehrlich, 2012). HD is caused by a CAG expansion mutation coding for the polyglutamine tract located in the N-terminal region of the huntingtin protein (HTT) (The Huntington's Disease Collaborative Research Group., 1993). At this time, there is no cure for HD or treatments to delay its onset and progression (Videnovic, 2013).

Standard HD models include transgenic animal models, immortalized rodent and human cell lines, and post-mortem tissue from HD patients (Bard et al., 2014; Lee et al., 2013). These models have been very useful in understanding some mechanisms behind HD pathogenesis; however, they do not fully represent human HD pathology (Kaye and Finkbeiner, 2013). Particularly important is the field's reliance on HD mouse models, which do not account for the potential to miss key drug targets, the effects of polymorphisms on human protein toxicity, human-specific cell subtypes, and transcription factor binding sites specific to humans. A promising complementary approach for modeling HD is the use of human induced pluripotent stem cells (iPSCs) derived from HD patient somatic cells (An et al., 2012; Zhang et al., 2010). HD iPSCs harboring mutant HTT protein (mHTT) have the potential to model the disease more accurately, as they are untransformed and capable of differentiating into multiple types of neural tissue. Human iPSCs also provide the advantage of following the progress of the disease during neural development and detecting early pathological changes—the presymptomatic stage. iPSCs provide a platform for systemic genomic profiling and drug screening and are a promising tool for cellular replacement therapy in HD patients.

We have previously established HD-patient-derived iPSCs and corrected their genetic defect through the use of homologous recombination-based gene targeting methods (An et al., 2012). Characterization of these isogenic lines and derivative neural precursors showed that correction of the expanded polyglutamine region to a non-disease causing length resulted in a normalization of cellular phenotypes consistent with several well-established and reproducible aspects of the disease—cell death, loss of brain-derived neurotrophic factor (BDNF) expression, and reduction of mitochondrial respiratory capacity, among other cellular phenotypes (An et al., 2012; Zhang et al., 2010). These phenotypes were apparent in differentiated neural stem cells (NSCs) but not the pluripotent stem cell fate. In a separate study, HD iPSCs displayed elevated lysosomal activity indicating a disruption in cellular maintenance and protein degradation (Camnasio et al., 2012). Finally, a study identified the key functional differences

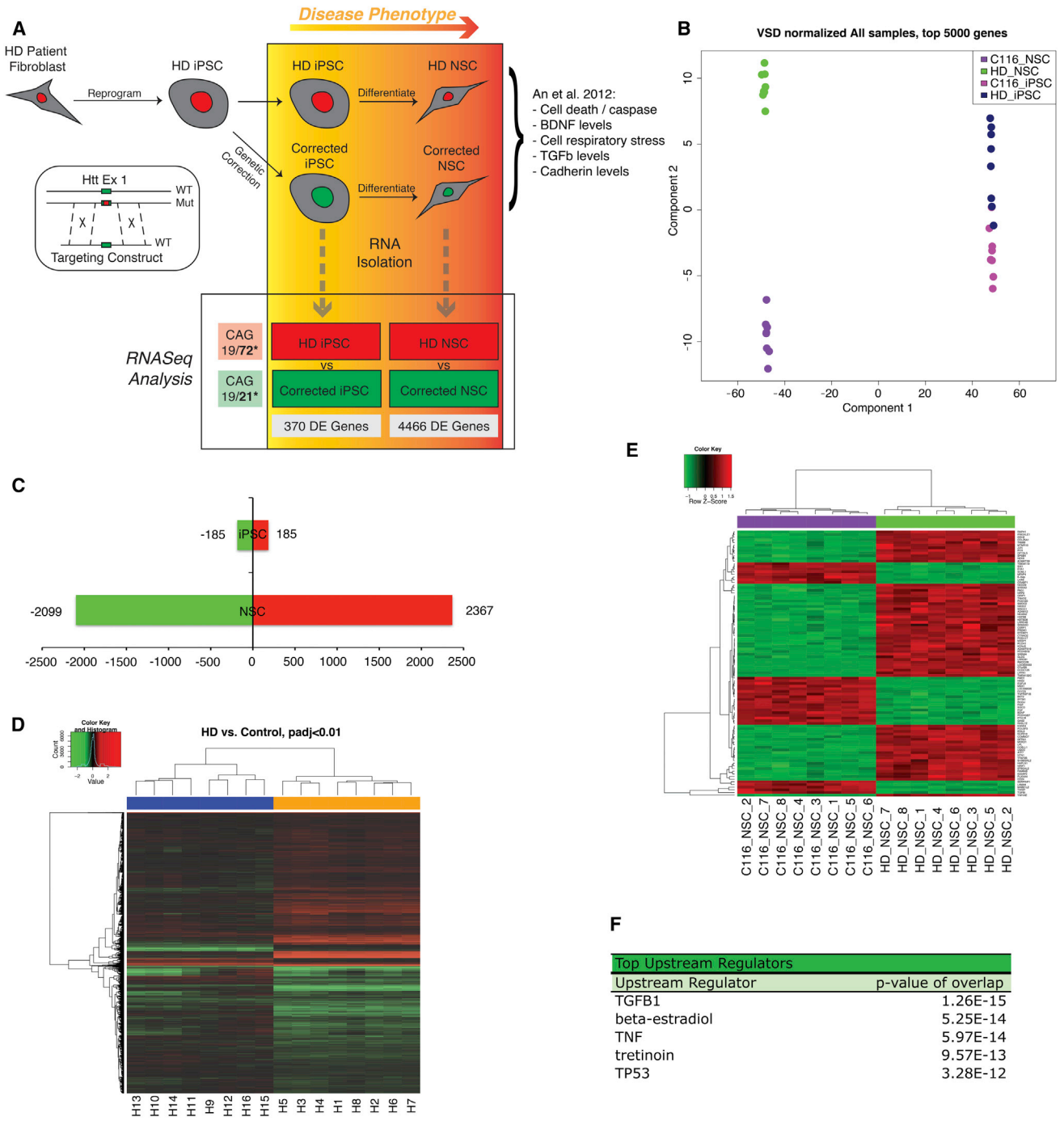

F

Top Upstream Regulators	
Upstream Regulator	p-value of overlap
TGFB1	1.26E-15
beta-estradiol	5.25E-14
TNF	5.97E-14
tretinoin	9.57E-13
TP53	3.28E-12

Figure 1. RNA-Seq Analysis of HD Isogenic Stem Cell Model

(A) Schematic illustration of experimental design and analysis. iPSCs reprogrammed from HD patient fibroblasts were genetically corrected for the *HTT* mutation using traditional homologous recombination via a targeting construct. Resulting isogenic iPSC pairs and differentiated isogenic NSC pairs were grown in tandem and plated as replicates for RNA isolation and RNA-seq analysis. There are eight biological replicates (BR) of each-corrected iPSCs, HD iPSCs, corrected NSCs, and HD NSCs: a total of 32 samples.

(B) Multi-dimensional scaling based on VSD-normalized expression levels of the top 5,000 most variable genes.

(C) Number of DE genes across comparisons at <0.01 false discover rate (FDR) threshold. Green bars represent the numbers of down-regulated genes and red upregulated for each comparison.

(legend continued on next page)

in striatal medium spiny neurons (MSNs) generated from HD and control patient iPSCs (HD iPSC Consortium, 2012). HD MSNs display altered electrophysiological properties including differences in their ability to fire spontaneous and evoked action potentials and to regulate intracellular calcium signaling.

Our initial endeavors in characterizing our isogenic iPSCs lines included a microarray-based large-scale gene expression analysis comparing the HD iPSCs with the corrected line C116 iPSCs (An et al., 2012). These studies were restricted to a comparison of only the iPSCs lines but yielded several useful insights regarding the biology of these established cell models. Specifically, we found that global gene expression remained essentially unchanged at the iPSC state upon analysis of isogenic pairs (HD iPSCs versus corrected iPSCs). We identify an order of magnitude fewer significantly differentially expressed (DE) genes when compared to a separate experiment, evaluating a non-isogenic pair of HD iPSCs versus normal iPSCs derived from an unrelated healthy individual, likely due to differences in genetic background as found in other studies (Fogel et al., 2014). The low degree of DE genes between corrected and uncorrected isogenic iPSCs supports several important points regarding the biological characterization of this HD model: (1) isogenic gene modification does not dramatically alter the expression profile of these cells, (2) *HTT* gene correction does not markedly alter gene expression at the iPSCs state—consistent with disease biology, (3) gene expression analysis in controlled isogenic cell line studies may represent a cleaner approach to discovery of disease-relevant pathway effects, and (4) further analysis in disease-affected cell types may allow the ability to resolve disease-specific coexpression traits unique to those cell types.

Here, we present transcriptomic and bioinformatic analysis of disease-relevant and non-relevant cell types in tandem with an isogenic human stem cell model of HD. DE analysis and weighted coexpression analyses confirmed the cell-specific nature of gene expression changes due to mHTT. We used weighted gene coexpression network analysis (WGCNA) to analyze the non-disease and disease states of our isogenic HD stem cell model and determine clusters of co-regulated genes, known as modules, that define each state (Langfelder and Horvath, 2008). The modules were analyzed by Genemania, functionally annotated by DAVID, analyzed by Enrichr, and the top, most connected transcripts (hubs) were studied in detail. Inclusion of HD iPSCs, which do not show a phenotype, enabled the isolation of coexpression traits specific to the HD NSCs and the identification of pathways involved in HD pathogenesis. Further modulation of key members of these signaling pathways rescued some HD disease phenotypes.

RESULTS

Analysis of Differential Gene Expression in Undifferentiated and Differentiated HD Induced Pluripotent Stem Cell Models

Previously, we characterized the genetically corrected lines of HD patient-derived iPSCs and found that a phenotype was apparent in the differentiated NSC stage but absent at the pluripotent stem cell state (Figure 1A) (An et al., 2012). We aimed to use this neural-specific correlation between disease genotype and disease phenotype to inform our global analysis of transcriptional changes that occur as a result of mHTT in our established human HD isogenic stem cell model (Figure 1A). Both iPSCs and NSCs were grown in tandem for three passages and eight replicates of each line were plated. Libraries were made from all 32 samples and sequenced using a HiSeq2000 sequencer to an average depth of 23.7 million 50 bp, paired-end reads per sample, 87% uniquely mapping to the human reference genome. Multidimensional scaling (MDS) showed distinct clustering of sample groups (Figure 1B). All iPSCs samples fall within a distinct cluster from NSCs samples. HD and corrected NSCs samples fall within distinct clusters dependent on the CAG length. By contrast, HD and corrected iPSC samples do not clearly delineate from each other. This is consistent with the distinct phenotypes found in HD NSCs and not HD iPSCs.

EdgeR was used to identify DE genes in each of the two paradigms (NSCs, iPSCs). We assessed the effect of HD mutation in both groups (HD iPSCs versus corrected iPSCs; HD NSCs versus corrected NSCs, false discovery rate threshold: 1%). We identified 4,466 DE genes when comparing HD NSCs and corrected NSCs, of which 2,367 were upregulated and 2,099 were downregulated in the disease state

(D) Heatmap representing DE genes in any of the comparisons of HD versus control. Samples (in columns noted H1–H16) and genes (in rows) are clustered by similarity. Shades of red represent upregulation, shades of green downregulation.
(E) Heatmap representing relative expression levels of the DE genes when comparing HD NSCs and corrected NSCs at an adjusted p value of <0.01. Gene names are listed on the right. The nomenclature is the NSC corrected line C116 and the sample number (C116_NSC_#) and HD-NSC and its corresponding sample number (HD_NSC_#).
(F) Table summary of top upstream regulators in HD versus corrected NSC samples via IPA analysis.
See also Tables S1 and S2.

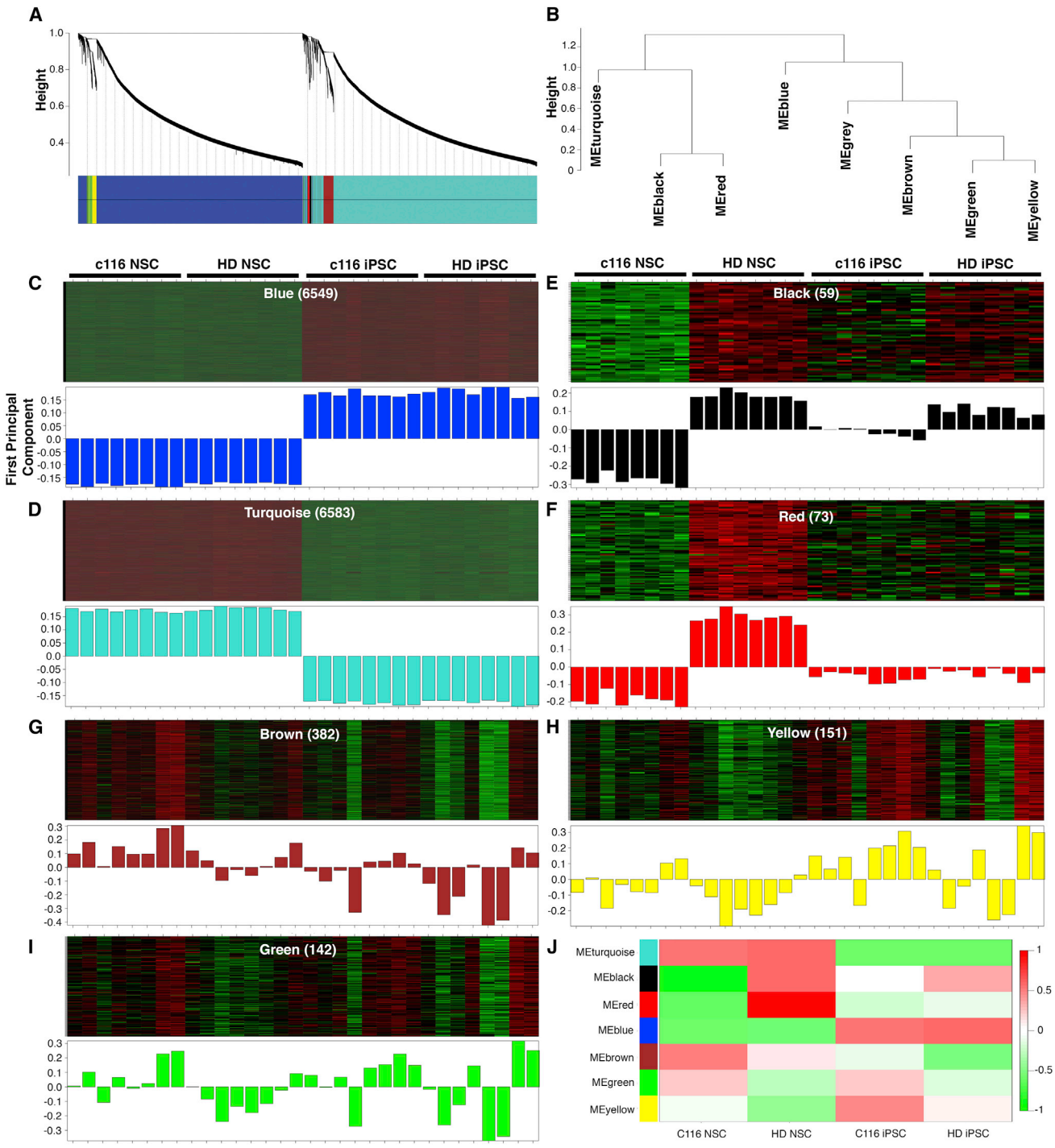

Figure 2. WGCNA Analysis of HD Isogenic Stem Cell Model Reveals Drivers of HD Phenotypes in NSCs

(A) Dendogram of genes clustered based on topological overlap. Identified modules are defined by colors.

(B) Dendrogram representing the seven modules identified by WGCNA. The gray module represents genes that are not included in any of the modules.

(C–I) Heatmap (top) and first principal component (eigengene, bottom) of expression data for genes in WGCNA modules across 32 samples. Samples are labeled by group, and the number of genes in each module is in parentheses. Of seven distinct modules defined, turquoise and blue modules are characterized by coexpression traits consistent with expression differences between the iPSC and NSC state (C and D),

(legend continued on next page)

(Figure 1C; Table S1). In contrast, only 370 genes were DE when comparing HD iPSCs to corrected iPSCs (Figure 1C; Table S1). This greater than 10-fold difference in globally DE genes in the disease/corrected NSC pair compared to the same cell pairs in the iPSC state correlates with the neural specific disease phenotypes in HD. Clustering of these DE genes across all samples shows discrete clusters of genes with distinct expression patterns between NSC and iPSC samples (Figure 1D). Functional annotation of the DE genes between HD NSCs and corrected NSCs groups are listed, representing the most significant changes in gene expression at the NSC state due to CAG repeat length (Figure 1E; Table S2). Functional annotation of the DE genes when comparing HD NSCs and corrected NSCs highlighted several gene ontology (GO) categories, including extracellular matrix organization ($p = 0.000027$), regulation of synapse assembly ($p = 0.000097$), mammalian phenotype-abnormal survival or perinatal lethality ($p = 2.8e\text{-}7$), and numerous genes involved in axonal guidance such as netrin-1, semaphorin 3D (SEMA3D), BDNF, and cadherin family members. Targets of the transcription factor SMAD3 were overrepresented ($p = 0.0018$), and the top WikiPathway was BDNF signaling ($p = 0.0053$).

Ingenuity Pathway Analysis (IPA) of the genes that are DE between HD NSCs and corrected NSCs highlighted, among the top upstream regulators, transforming growth factor β (TGF-β), β-estradiol, and tumor necrosis factor alpha (TNF-α) (Figure 1F). TGF-β is particularly interesting as it plays a critical role in temporal neurogenesis where the onset of TGF-β signaling determines the overall lifespan of the temporal lineage (Dias et al., 2014). HTT is required for neurogenesis and mHTT disrupts striatal and cortical neuronal development (Molina-Calavita et al., 2014; Molero et al., 2009). The role of TGF-β has not been investigated extensively in HD but has been in other neurological diseases, such as Alzheimer's disease and Parkinson's disease, where levels of this factor are elevated (Vawter et al., 1996; Zetterberg et al., 2004). Levels of TGF-β are altered in cortical neurons and in peripheral blood of HD patients, as well as in mouse models of HD (Battaglia et al., 2011; Kandasamy et al., 2011). Microarray and bioinformatics analysis of a HD neuronal *Caenorhabditis elegans* model revealed Wnt/TGF-β as relevant to pathogenesis (Tourette et al., 2014). Similarly, a link with β-estradiol has not been well studied, but it has been shown that male HD transgenic rats display decreased levels of 17β-estradiol at older ages (Bode et al., 2008). Lastly, HD is associated with increased levels of proinflammatory cytokines such as TNF-α, suggesting a role in inflammatory response, which may contribute to HD progression (Björkqvist et al., 2008; Hsiao et al., 2014).

Network Analysis Reveals Modules of Genes Associated with the Pathogenic CAG Repeat

We chose to take advantage of the multi-differentiated state of our experimental design by implementing a coexpression network analysis that could further inform our understanding of the biology of HD. WGCNA was performed on the full RNA sequencing (RNA-seq) expression data across the four distinct cellular states (32 samples) (Figure 1A). WGCNA identifies modules of coexpressed genes that reflect shared functions or cellular components. In addition, identification of highly connected genes (hubs) allows us to pinpoint genes and pathways relevant to further analysis. WGCNA revealed seven distinct modules representing highly co-expressed networks of genes (Figures 2A and 2B; Table S3). A module first principal component (eigengene) can be used to visualize the expression levels for each module across the 32 samples. This analysis showed that some modules (blue, turquoise) represented differences across cell types, whereas for others (red, black), the eigengene was correlated primarily with genotype (Figures 2C–2J).

We used DAVID to assess the GO annotation of each module (Table S4). The two largest modules by size, blue and turquoise, represent expression changes that clearly delineate between NSC and iPSC sample groups, strongly reflecting expression differences between the iPSC and the differentiated NSC states (Figures 2C, 2D, and 2J). Top biological processes associated with the blue module (downregulated in NSCs relative to iPSCs) include translation, metabolic process, ribosome biogenesis, and proteasomal catabolic process, while conversely, processes associated with the turquoise module (upregulated in NSCs relative to iPSCs) include regulation of transcription, DNA-dependent chromatin modification, chromosome and chromatin organization, cell cycle, and response to DNA damage (Table S4).

We further identified two coexpression modules with features highly relevant to the HD phenotype (Figures 2E and 2F). We hypothesize that the genes in these modules would be more closely relevant to HD as we observe a relevant phenotype in neuronal states and less difference in pluripotent stem cell states. The black (59 genes) and red (73 genes) modules represent genes that are highly upregulated in HD NSCs, while expression differences between HD and

whereas other individual modules define expression profiles consistent with changes in gene expression in NSCs due to CAG expansion (E and F) y axis is first principal component for (C)–(I).
(J) Summary of all modules by sample group.
See also Tables S3, S4, S5, and S6.

control are less pronounced in the iPSC state (Figures 2E, 2F, and 2J). Functional annotation highlighted differences in the biological processes (GO terms) associated with gene members of the red and black modules. Most significant biological processes in the red module include enriched terms neuron differentiation, neuron development, morphogenesis, axonogenesis and axon guidance, whereas no terms were significantly associated with the black module after multiple testing correction (Table S5). The remaining three modules, brown, yellow, and green, (Figures 2G–2I) showed modest correlation with either the cell type or the genotype.

Identifying the Top Genes within the Consensus Modules Based on Significance and Fold Change

Having identified two modules of interest with regard to cell-type-specific gene expression changes due to mHTT, we further focused on the members of these two groups and the gene expression fold changes at the NSC state (HD versus corrected). At a p value cutoff of <0.01, all members of the black module, and all but one in the red module are below that threshold (Table S6). A volcano plot of red and black module members allows further visualization of the highly significant genes in these two groups, while also identifying large magnitude fold changes from these groups (Figure 3A). A log2 fold change cutoff of 1 is shown (Figure 3A; Table S6). Genes that we found upregulated in HD NSCs compared to controls were *NTN1*, *CDH2*, *DPYSL5*, *CTNND2*, *YWHAE*, *C7orf29*, *LRRC61*, *LRRC4B*, *SEMA3D*, *PCDHB15*, *PCDHB18*, *UQCC*, *SPOCK3*, and *GRIP1*.

Identification of Hub Genes in the Modules

Next, we focused on the genes with the highest intramodular connectivity (hub genes), as these are the best representative of the expression of the entire module (Langfelder et al., 2013) and may represent points of biological interest in defining the HD phenotypes. Network plots for the red and black modules, highlighting the top most connected genes, are represented in Figures 3B and 3C (Figures S1A–S1E show the other modules).

For the red module, four hub genes were identified: *SEMA3D*, *CDH2*, *IRS1*, and *APBB2* (Figure 3B). Semaphorins are a class of secreted and membrane proteins that act as growth cone guidance molecules through the receptors plexins and are coupled to RRAS. Previously, we identified RRAS as a therapeutic target for HD using a siRNA screen to the druggable genome (Miller et al., 2012). Semaphorin 4D inhibition was shown to ameliorate neuropathology and some cognitive deficits in HD mouse models (Southwell et al., 2015). Cadherin has been linked directly to the function of the HTT protein (Lo Sardo et al., 2012). The HTT protein evolved to acquire a unique regulatory activity for controlling neural adhesion via ADAM10-N-cadherin. Mouse striatal neurons expressing mHTT have altered N-cadherin levels and neuritogenesis (Reis et al., 2011). Insulin growth receptor substrate 1 (*IRS1*) has not been investigated in HD, but mice lacking this protein are long-lived and lack many of the diseases of aging (Selman et al., 2008). Finally, the amyloid-β precursor protein-binding, family B, member 2 (*APPB2*) is involved in APP processing and levels of phosphorylation (Sakuma et al., 2009).

For the black module, eight hub genes were identified: *HSPB8*, *DOK5*, *SH3BGRL2*, *VGLL3*, *LYN*, *GRIP1*, *FAM131B*, and *EFEMP1* (Figure 3C). A few of these hub genes particularly stand out with respect to HD. AMPA receptors generate intracellular signals from the cell surface to the nucleus through the Lyn-MAPK pathway, which may contribute to synaptic plasticity by regulating the expression of BDNF (Hayashi et al., 1999). SH3BGL2 (intersectin 2) is involved in clathrin-mediated endocytosis and is a partner of dynamin (Evergren et al., 2007). DOK5 is a substrate for TrkB and TrkC receptors (Shi et al., 2006). Genemania network analysis of black and red modules are shown in Figures 3D and 3E highlighting the genes interconnections.

Enrichment Analysis of the Modules

As an alternative approach to rank and visualize enriched terms, we used the web-based gene list enrichment analysis tool Enrichr. Enrichr tools were applied to all seven modules (Table S6). We found that the genes of the black module are statistically enriched for genes associated with the mouse gene atlas term dorsal striatum (Figure 4A). We used GeneMANIA, a gene function tool that allows visualization between these genes with respect to coexpression, co-localization, and protein interaction to generate an annotated Cytoscape network for the black module (Figure 4B). We found *DARPP-32* to be associated with a number of these enriched networks. *PPP1R1B* (*DARPP-32*) is downregulated in NSCs but not iPSCs in our RNA-seq data, and differential expression of *DARPP-32* has been confirmed by qPCR analysis (Figure 4C) in distinct NSC cultures. DARPP-32 is an abundant protein expressed in striatal MSNs and its expression levels decrease in HD mouse models and human postmortem tissue.

Given the black module's enrichment to the mouse striatum, we next evaluated if this module is associated with the human striatum during development. We evaluated if any of the HD-relevant modules were enriched for striatum-specific marker genes identified from a genome-wide adult brain mouse atlas (Lein et al., 2007). While the top 100 genes with the most striatum-specific expression were selected, only 49 of these were actually expressed in our dataset. From the 50 mouse homologous genes in the black module, only *Dach1* is among the most striatum-specific

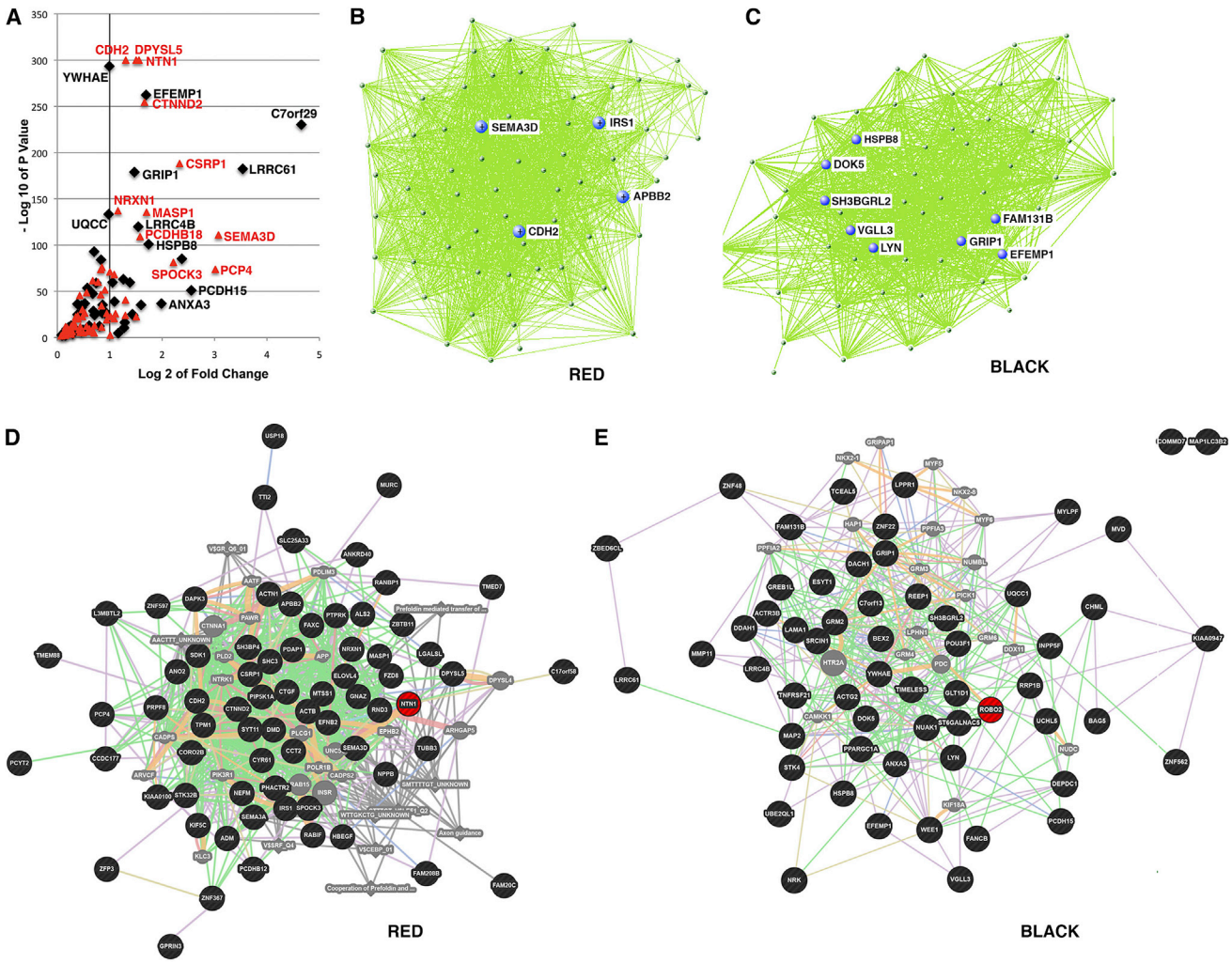

Figure 3. Volcano and Hub Connectivity of Module Genes, Visualized for the Red and Black Modules

(A) Volcano plot of genes in the red and black WGCNA modules, at $p < 0.1$. Individual top fold change genes are labeled.

(B and C) Network plot depicting the top connections for each module. Most highly connected module members (hub genes) are shown for each group.

(D and E) Genemania network analysis diagram of red and black modules. All module members in black, with genes of interest highlighted in red.

See also Figure S1.

marker genes, while there was no overlap with the 61 mouse homologous genes in red module. We also evaluated if the black or red modules were enriched for genes associated with human striatum during development, identified from gene expression data in prenatal human striatum (from 2 to 20 weeks of age) (Onorati et al., 2014). We found that the red module was statistically enriched for DE genes found to be upregulated in the developing human striatum (*ELOVL4*, *KIF5C*, *MTSS1*, *NEFM*, *NRXN1*, *NTN1*, *PCP4*, *STK32B*, and *TMEM88; Z* score = 4.18). Using WGCNA analysis, the group also identified a module, named M25, whose members are highly expressed in the developing human striatum (Onorati et al., 2014). We found that the black and red modules were statistically enriched for genes found in the M25 module (Figure 4D). The genes matching the highly expressed genes in the striatum were *BEX2*, *C7orf13*, *FAM131B*, *GREB1L*, *GRM2*, *LPPR1*, *LYN*, *MAP2*, *MMP11*, *MVD*, *NUAK1*, *POU3F1*, *PPARGC1A*, *SH3BGRL2*, *SRCIN1*, *TNFRSF21*, and *UQCC*. In addition to the black module, we also evaluated other key striatal-specific genes identified in the Onorati study using our RNA-seq expression dataset (Table S1). Well known genes in human striatal development *CTIP2*, *DARPP-32*, *ISL1*, *TBR1*, *FOXP1*, and *PAX6* are all downregulated in HD

A

Black Module Enrichment Term: Mouse Gene Atlas	P-value	Z-score	Comb. Score	Genes
dorsal_striatum	0.022	-1.943	1.427	UCHL5;DACH1;ROBO2;ACTR3B;POU3F1
olfactory_bulb	0.014	-1.923	1.412	GRIP1;LRRC4B;PPARGC1A;BAG5;GRM2;ROBO2;UBE2QL1
cerebral_cortex_prefrontal	0.042	-1.651	0.807	FAM131B;SRCIN1;UBE2QL1
eyecup	0.282	-2.502	0.678	PCDH15;HSPB8;DACH1;GREB1L
ciliary_bodies	0.158	-1.868	0.506	GREB1L;EFEMP1;DACH1
retina	0.185	-1.831	0.496	PCDH15;GRIP1;UCHL5
amygdala	0.151	-1.594	0.432	ST6GALNAC5;DOK5
nih_3T3	0.110	-1.532	0.415	FANCB;EFEMP1
MEF	0.145	-1.472	0.399	DDAH1;VGLL3;NUAK1
skeletal_muscle	0.211	-1.285	0.348	HSPB8;MYLPF;UQCC

B

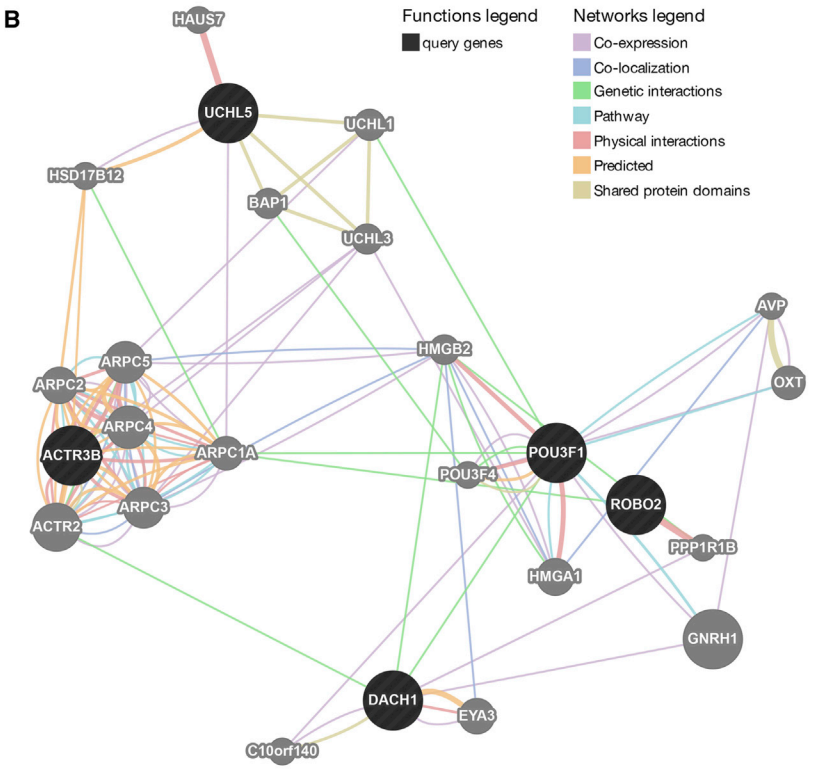

C

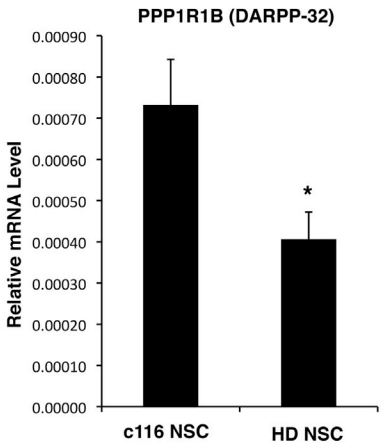

D

MODULE	# Official Gene Symbols	# Match to Module M25	Percent Match	Hypergeometric p-value
Black	59	19	32.20	1.26E-02
Red	73	25	34.25	1.82E-03
Brown	382	68	17.80	7.89E-01
Green	142	20	14.08	9.58E-01
Grey	13	0	0.00	1.00E+00
Yellow	151	19	12.58	9.89E-01
Turquoise	6584	1449	22.01	9.56E-12
Blue	6549	1304	19.91	6.19E-02

Number protein coding genes (From Human ENCODE paper): 20,687
Number of M25 genes from Onorati 2014 paper: 3989

Figure 4. The Black Module Is Linked to Expression of Genes in the Striatum

(A) Gene enrichment of black module gene members shows significant enrichment of genes associated with dorsal striatum based on the Mouse Gene Atlas list using the Enrichr tool.

(B) Subsequent visualization of networks associated with these five genes using the Genemania tool.

(C) qPCR analysis of *DARPP-32* mRNA levels in HD and C116 NSC samples (n = 5 BR). Five independent BR are displayed as mean ± SD.

(legend continued on next page)

NSCs compared to control NSCs (Figure S2). Interestingly, *FOXP2* is upregulated in HD NSCs compared to control NSCs, and its expression becomes more restricted in the human striatum during development (Onorati et al., 2014).

Because degeneration of MSNs is the pathological hallmark of HD, we used three independently generated lists of MSN-enriched gene sets, by laser-captured HD patient MSNs (Hodges et al., 2006), tagged ribosome profiling in adult mice (Heiman et al., 2008) and by FACS-sorting of D1/D2 MSNs (Lobo et al., 2006) for analysis. We found that in the red module, 16 of the 61 mouse homolog genes were MSN-specific marker genes, though the enrichment was not significant (*Z* score = 2.03). Moreover, the red module also included *NRXN1*, one of the nine genes differentially enriched in striatonigral (D1) neurons (Lobo et al., 2006).

We note that our coexpression modules identified highly upregulated genes at the HD NSC state in the black and red modules compared to control NSCs. Coexpression modules representing highly downregulated genes at the HD NSC state were not identified by the WGCNA analysis (Figure 2J). In particular, reduced expression of BDNF is a well-characterized phenotype in HD models and in brains of HD patients. BDNF is downregulated in HD NSCs in our RNA-seq analysis, and as noted above, BDNF signaling is the top Wikipathway identified among the 100 top DE genes ($p = 0.0053$). Using a hierarchical clustering approach, we identified genes whose expression pattern follows that of BDNF (Figure S3A). This cluster contains genes that, while unchanged in iPSCs, are downregulated in HD-NSCs compared to control NSCs and may therefore represent genes that are dysregulated in the NSC lineage of HD patients. It included several genes known to be associated with HD and striatal development, such as *BDNF*, *TGM2*, and *DARPP-32*, as well as five cadherins (*CDH15*, *CHD6*, *PCDHGA3*, *PCDHGB7*, and *PCDHGC4*) (Figure S3B). Genemania shows the coexpression network for this cluster of genes (Figure S3C). Enrichr links this module to dorsal striatum as well, and genes are enriched for the M25 module (Onorati et al., 2014). Further, this group contains a key constituent of the TNF upstream regulatory pathway that was identified in our IPA analysis of DE genes (Figure 1F): *TNFRSF1B* (*TNFR-II* or *p75*), whose expression highly correlates with BDNF. Based on these findings, we evaluated if the black or red modules were enriched for genes-associated BDNF depletion, identified from gene expression striatal profiles from BDNF knockout mice (Strand et al., 2007). We found that the red module was statistically enriched for genes upregulated (five genes: *CSRP1*, *NTN1*, *PCYT2*, *PTPRK*, and *SEMA3A*; *Z* score = 4.2) and downregulated (five genes: *ACTN1*, *GNAZ*, *HBEGF*, *PCP4*, and *TPM1*; *Z* score = 5.03) in the BDNF-KO mice.

We next tested whether genes in HD-associated modules were enriched for transcription factor binding sites using the ENCODE chromatin immunoprecipitation sequencing (ChIP-seq) significance tool (Auerbach et al., 2013). We found that both HD modules were enriched for the *Ezh2* (Enhancer of zeste homolog 2) factor, with 21 (out of the 58 valid) black module genes (Q value = 3.204e-2) and 28 (out of 65 valid) red module genes (Q value = 5.905e-5) having a binding site for this particular transcription factor. EZH2, is the functional enzymatic component of the polycomb repressive complex 2 (PRC2), which is involved in various biological processes, including differentiation, maintenance of cell identity and proliferation, and stem-cell plasticity (Margueron and Reinberg, 2011). HTT facilitates PRC2 function and this is at least partially mediated by the physical interaction of full-length wild-type HTT protein with the Ezh2 and Suz12 PRC2 core component (Seong et al., 2010).

Therapeutic Targets Can Be Identified from Bioinformatic Analysis of Expression Data from HD NSCs

Bioinformatics analysis revealed key signaling molecules in neurogenesis, striatal development and axonal guidance. Consistent with this, two pathways identified relevant to HD phenotypes include TGF-β (top altered RNA-seq pathway) and netrin-1 (black module). Both of these pathways are required for neurogenesis and are linked to development of the striatum. Therefore, we evaluated whether these pathways were altered in our HD NSC model and if modulation was neuroprotective.

TGF-β is the top signaling pathway that is altered between HD and corrected NSCs based on our RNA-seq results. Therefore, we evaluated TGF-β signaling in our human HD stem cell model and in zQ175 knockin HD mice. First, we determined basal levels of TGF-β expression in HD and corrected NSCs. TGF-β is part of a larger complex and appears in multiple forms including its precursor form (~60 kDa), its active dimer form (~24 kDa), and its inactive monomer form (~12 kDa) (Annes et al., 2003). Using a pan-TGF-β antibody that recognizes all three TGF-β isoforms, western blot analysis of HD and corrected NSC lysates revealed that HD NSCs significantly express more TGF-β in its precursor, dimer, and monomer forms (Figures 5A

(D) Both the red and black modules have genes enriched for human striatum. The matches for the red module are *ACTB*, *C17orf58*, *CORO2B*, *CTNND2*, *FAM20C*, *GNAZ*, *GPRIN3*, *HBEGF*, *KIF5C*, *MTSS1*, *MURC*, *NEFM*, *NRXN1*, *NTN1*, *PCDHB12*, *PCDHB18*, *PCP4*, *RAB1F*, *RND3*, *SDK1*, *STK32B*, *TMEM88*, *TPM1*, *TUBB3*, and *ZN597*.
See also Figures S2 and S3.

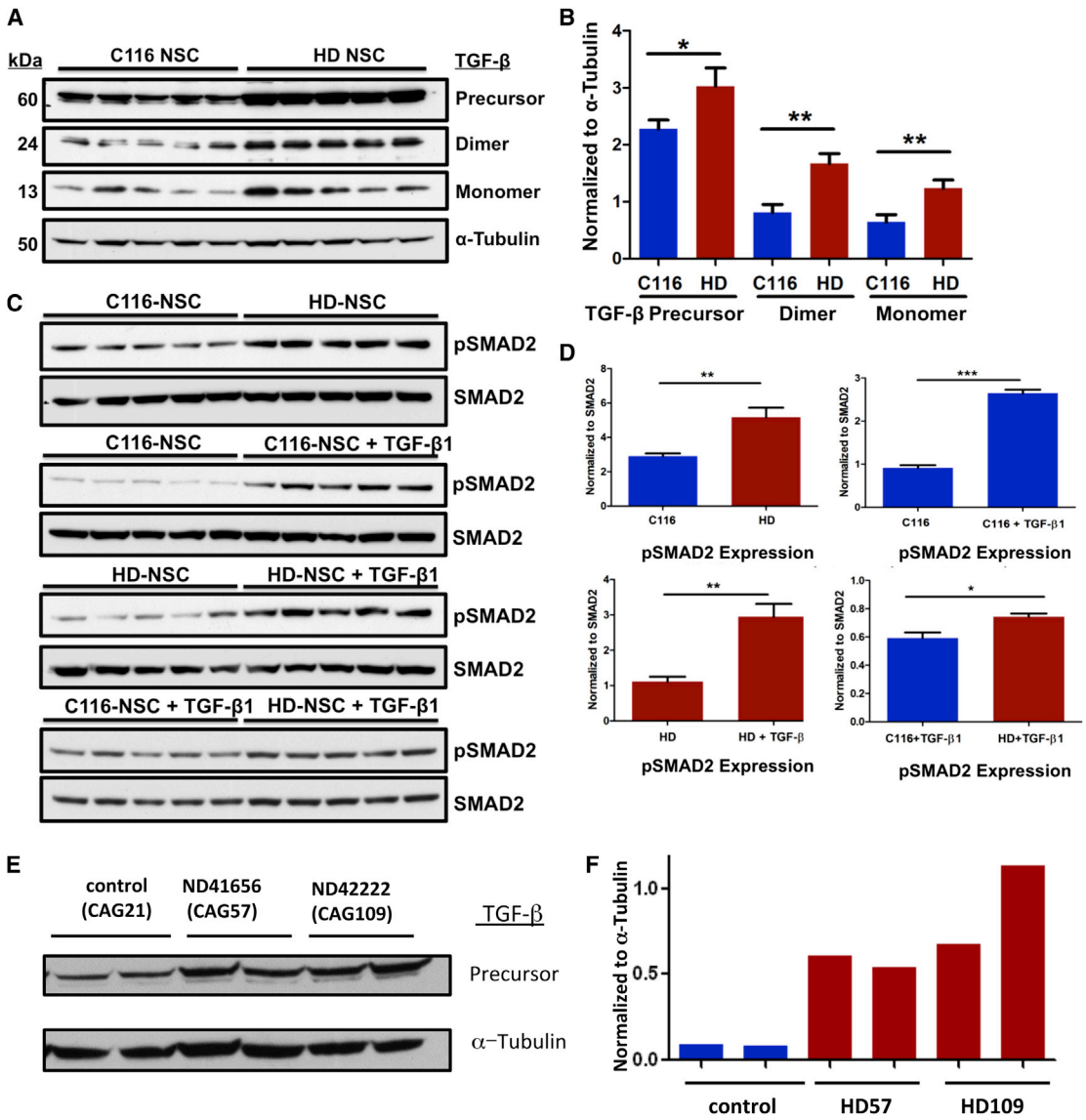

Figure 5. TGF-β Expression and SMAD Signaling Is Altered in HD NSCs

(A) TGF-β protein levels in HD (n = 5 BR) and corrected C116 NSCs (n = 5 BR) were determined by western blot and normalization to α-tubulin.

(B) HD NSCs had elevated TGF-β protein in multiple forms including the TGF-β precursor complex, TGF-β dimer and monomer, compared to C116 NSCs.

(C) SMAD activation, indicated by phosphorylation of SMAD2 (pSMAD2), was determined in HD and C116 NSCs via western blot by normalization to SMAD2.

(D) Both corrected and HD NSCs activated the SMAD signaling pathway upon treatment with recombinant human TGF-β1 (10 ng/ml) for 1 hr. Under normal basal conditions, HD NSCs have higher levels of activated pSMAD2 compared to corrected NSCs. Similarly, HD NSCs treated with TGF-β1 had higher levels of pSMAD2 compared to C116 NSCs. All experiments had five biological replicates per genotype, and each experiment was repeated three times.

(E) TGF-β protein levels in HD lines (n = 2 BR) and control NSCs (n = 2 BR) were determined by western blot and normalization to α-tubulin.

(F) Densitometry of the western blot shown in (E).

and 5B). TGF-β ligands signal through TGF-β receptors and activate SMAD proteins through phosphorylation of SMAD2/3 (Dennler et al., 2002). Because TGF-β1 expression is increased in the brain in response to injury (Krupinski et al., 1996), we determined whether recombinant TGF-β1 could modulate TGF-β signaling in HD NSCs and

ameliorate HD phenotypes. To test for activation of SMAD signaling, HD and corrected NSCs were treated with or without TGF-β1. Both corrected and HD NSCs showed an increase in pSMAD2 levels upon TGF-β1 treatment compared to untreated NSCs (Figures 5C and 5D). In basal conditions without TGF-β1 treatment, HD NSCs expressed more pSMAD2 than corrected NSCs. Furthermore, TGF-β1 treatment resulted in higher pSMAD2 phosphorylation expression in HD NSCs compared to corrected NSCs. Thus, both HD and corrected NSCs can activate SMAD signaling upon exposure to TGF-β1, however HD NSCs have more pSMAD2 overall. This could be due to HD NSCs having more TGF-β or to a compensatory mechanism to combat the HD mutation. To confirm that expression of TGF-β changes are observed in multiple patient HD iPSC lines (nonisogenic), we also analyzed HD iPSC lines ND41656 (CAG57) and ND42222 (CAG109) and compared them to a control (Figures 5E and 5F). We found that the levels of TGF-β were higher in NSCs derived from the HD lines compared to the control.

Elevated levels of TGF-β protein and changes in TGF-β signaling in HD suggest a potential neuroprotective role for TGF-β in the brain. Therefore, we determined whether TGF-β1 could rescue HD-related phenotypes that we identified in our earlier studies (An et al., 2012; Zhang et al., 2010). We previously found that HD NSCs had elevated caspase-3/7 activity compared to corrected NSCs upon removing serum from cell culture medium. To determine if TGF-β is protective in a toxicity assay, we cultured corrected or HD NSCs in either (1) their regular NSC media supplemented with growth factors (complete), or (2) in basic medium without growth factor but supplemented either with recombinant TGF-β1 or TGF-β2 for 48 hr. Both TGF-β1 and TGF-β2 significantly reduced caspase-3/7 activity in basic conditions (Figure 6A). The reduction in caspase activity occurred in a dose-responsive manner (Figure 6B), as higher concentrations of TGF-β1 were more effective at reducing caspase activity in HD NSCs in basic conditions. We did not see a significant reduction in caspase activity in corrected NSCs in basic conditions with addition of either TGF-β1 or TGF-β2. We also evaluated whether the deficit in maximal respiratory capacity in HD NSCs was normalized by TGF-β1 treatment. HD NSCs have deficits in mitochondrial function when compared to corrected NSCs as measured by Seahorse respiration (An et al., 2012). TGF-β1 treatment rescued the respiratory deficit in HD NSCs (Figure 6C).

After confirming that TGF-β protein levels and SMAD signaling are altered in HD NSCs, we next asked whether TGF-β levels are also altered in vivo. We analyzed the cortex and striatum of zQ175 HD knockin mice for TGF-β expression at 6 and 12 months of age. In the cortex, zQ175 homozygous mice had elevated levels of multiple TGF-β protein forms compared to wild-type littermate controls. Specifically, zQ175 cortex at 6 months had significantly higher levels of the TGF-β precursor and dimer and exhibited a trend in having more TGF-β monomer compared to controls. At 12 months, zQ175 cortex had higher levels of TGF-β dimer and showed a trend toward having more TGF-β monomer when compared to controls (Figure 6D). Results were not as conclusive for the striatum (Figure 6E). We only observed a significant increase in TGF-β monomer in zQ175 mice when compared to controls at 12 months of age (Figure 6D). Our zQ175 results support our in vitro findings and suggest that TGF-β expression is elevated in HD brains.

Next, we investigated if modulation of the genes in the red module would have a neuroprotective effect in our HD NSC model. We focused on the axonal guidance molecule netrin-1 (Figures 3A and 3D) since it was one of the most significantly altered genes in this module that has defined function in the axonal guidance pathway. Furthermore, netrin-1 is expressed in the striatal ventricular zone during development, guides the large influx of striatal matrix neurons into the striatum, and is critical to the formation of fundamental striatal structures (Hamasaki et al., 2001). As shown in Figures 7A and 7B, the receptors for netrin-1, such as DCC and UNC5D, have increased expression in HD NSCs as determined by qPCR (Figure 7B). Elevated levels of netrin-1 and changes in this signaling pathway in HD may suggest a potential neuroprotective role for netrin-1 in the brain. To test this, we treated HD NSCs with recombinant netrin-1. We found that netrin-1 treatment reduced caspase-3/7 activity in growth factor starved HD NSCs and is potentially neuroprotective (Figure 7C). We also evaluated whether the deficit in maximal respiratory capacity in HD NSCs was normalized by netrin-1 treatment. Netrin-1 treatment rescued the respiratory deficit in HD NSCs (Figure 7D). The netrin protein levels were not significantly altered in the zQ175 mice at 12 month of age compared to controls as measured by western blot analysis (data not shown). Perhaps the alteration occurs early in development and is normalized in adults.

DISCUSSION

In our previous work, we found cellular and molecular phenotypes associated with HD in NSCs derived from HD patient-specific iPSCs when compared to isogenic controls. The phenotypes we reported included susceptibility to cellular death as measured by caspase activity and TUNEL staining, mitochondrial deficits, lower levels of BDNF, altered cadherin and TGF signaling (An et al., 2012). The cellular and molecular phenotypes were only associated with the differentiated HD NSC state and were not detected

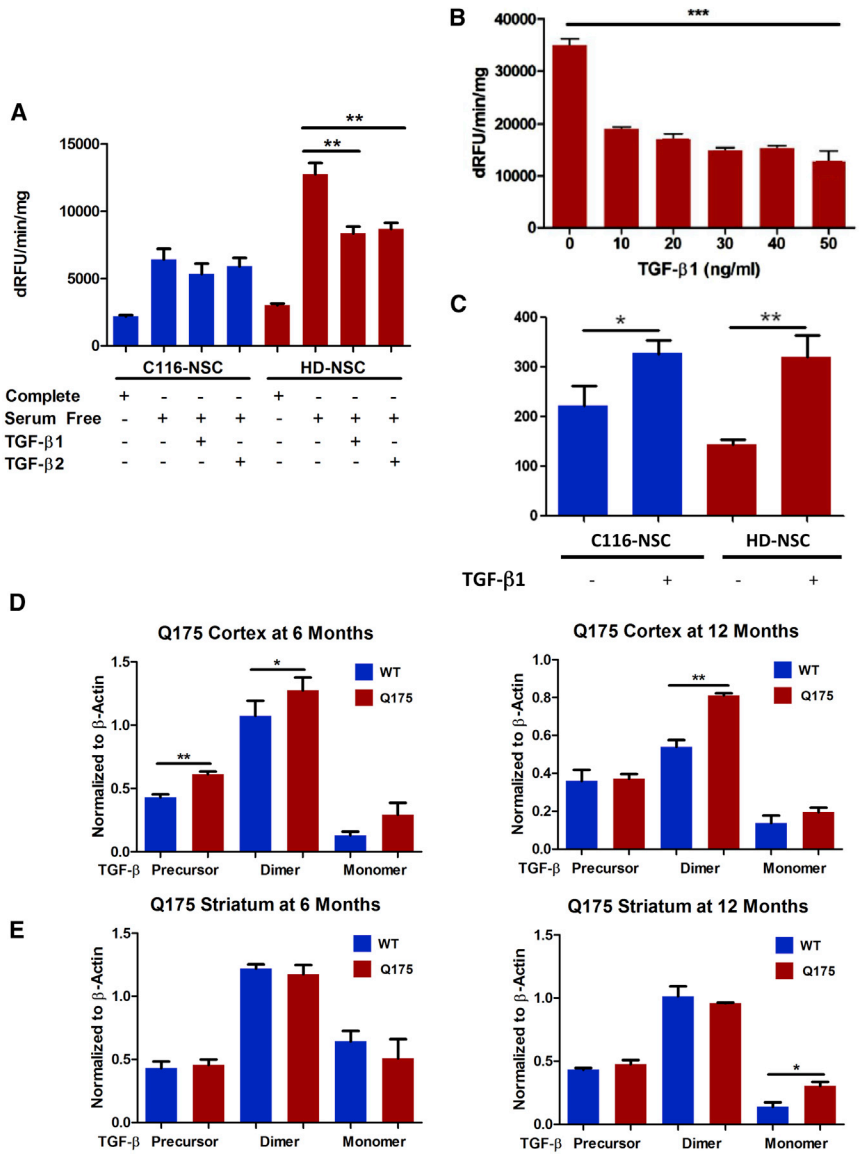

Figure 6. TGF-β Expression Has Neuroprotective Effects In Vitro and Is Elevated In Vivo

(A) HD NSCs have elevated caspase-3/7 activity upon growth factor withdrawal. This phenotype is partially rescued by treatment with either recombinant human TGF-β1 or TGF-β2 (10 ng/ml) (n = 5 BR per genotype, each experiment repeated three times).

(B) TGF-β1 ameliorates elevated caspase-3/7 activity in HD NSCs in a dose response manner (n = 5 BR per genotype).

(C) Maximal respiratory capacity of HD NSCs and C116 NSCs was measured in the presence and absence of TGF-β (N = 6 BR per genotype, each experiment repeated three times).

(D) TGF-β expression in the cortex of zQ175 mice at 6 months was higher in the precursor and dimer forms and higher in the dimer form at 12 months of age (n = 3 BR per genotype, each experiment repeated three times).

(E) In the striatum, TGF-β monomer was elevated in zQ175 compared to wild-type at 12 months, but no significance was seen at 6 months (n = 3 BR per genotype, each experiment repeated four times).

in HD iPSCs. This finding suggests that the first disease phenotypes in HD manifest during early development at the NSC stage. This is interesting because we may be detecting HD developmental changes that occur early in disease progression, in our human HD NSC models.

To examine the molecular basis of the phenotypes found in HD NSCs, we used RNA-seq to measure expression changes in these cellular states. Inclusion of HD iPSCs, which do not show a distinct disease-associated phenotype, enabled specific isolation of coexpression traits specific to the HD NSCs and the identification of pathways involved in HD pathogenesis. WGCNA analysis revealed the effects of HTT CAG expansion on NSCs and identified two modules driving HD phenotypes—the black and red modules. By studying gene expression changes in prenatal human striatum during development, using WGCNA analysis, another group identified a module they named M25 whose members are highly expressed in the developing human striatum (Onorati et al., 2014). We found that the black and red modules were enriched for genes found in the M25 module, which is associated with human striatal tissue. In addition to the black and red module, we also evaluated other key striatal-specific and well known genes in human striatal development including *CTIP2* (*BCL11B*), *DARPP-32* (*PPP1R1B*), *ISL1*, *TBR1*, *FOXP1*, and *PAX6*, which were all downregulated in HD NSCs compared to control NSCs. This is consistent with a number of studies showing mHTT alters cortical and striatal neurogenesis in mouse models of HD (Molero et al., 2009), and the normal function of HTT is implicated in neurogenesis.

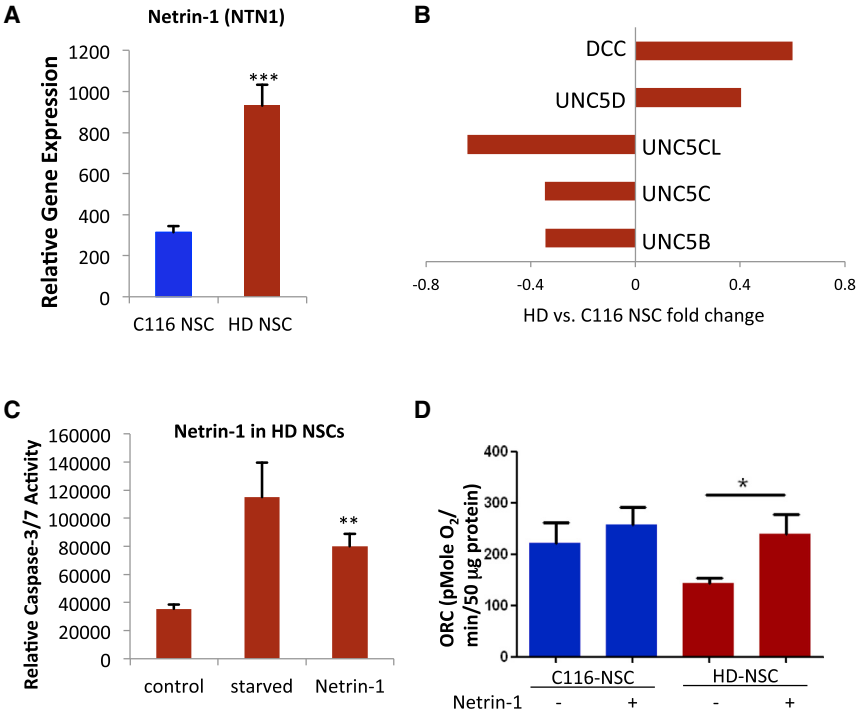

Figure 7. Netrin-1 Is Neuroprotective in HD Stem Cell Model

(A) The expression of netrin-1 mRNA in increased in HD NSCs (n = 8 BR per genotype, repeated three times).

(B) The receptors for netrin signaling have altered expression in HD NSCs (n = 8 BR per genotype).

(C) HD NSCs have elevated caspase-3/7 activity upon growth factor withdrawal. This phenotype is rescued by treatment with netrin-1 (100 ng/ml) (n = 5 BR per condition, repeated three times).

(D) Maximal respiratory capacity of HD NSCs and C116 NSCs was measured in the presence and absence of netrin-1 (n = 6 BR per genotype, repeated three times).

Indeed, knockin HD mice with Q111 repeats exhibited delayed striatal cytoarchitecture with altered expression of markers of MSNs (Molero et al., 2009). The role of development in neurodegeneration has been addressed in a related polyglutamine expansion disease, SCA1 (Serra et al., 2006). When ATXN1[82Q] expression in SCA1 mice was delayed during postnatal development, the disease was less severe. This correlation of genes found in our NSC analysis and in previous mouse studies in the field support the concept that NSCs can be a valuable tool for modeling a disease in a dish.

A question arising from this work is whether development sets the stage for the early pathophysiological abnormalities in HD and whether we can identify candidate pathways or genes that will restore neuronal homeostasis and protect striatal MSNs halting disease progression. We believe the black and red modules defined in our studies represent critical cellular pathways that are disrupted in early HD pathogenesis and that normalization will restore neuronal homeostasis and prevent neuronal degeneration. Our bioinformatics analysis revealed key signaling molecules in neurogenesis, striatal development, and axonal guidance for these modules. To test whether these pathways were altered in HD and represented therapeutic targets for HD, we focused on two signaling pathways: TGF-β and netrin. During development the striatum forms from the ventral telencephalon and is dependent upon BMP/TGF-β inhibition (Kuang et al., 2006) as well as netrin-1 signaling (Hamasaki et al., 2001). Our studies of TGF-β signaling in HD reveal that this signaling pathway is altered in HD. Both HD NSCs and HD knockin mouse brains express more TGF-β than wild-type controls. Furthermore, TGF-β1 is neuroprotective in our NSC models and can ameliorate some HD phenotypes including reducing caspase activity and improving respiratory capacity in HD NSCs. These results suggest a possible compensatory mechanism in which HD NSCs express higher levels of TGF-β in order to compensate for the negative effects caused by the HD mutation. Our findings show that netrin-1 levels and receptors were altered in HD NSCs. The addition of axonal guidance molecule was neuroprotective consistent with the neuroprotective role of netrin-1 after stroke (Liao et al., 2013). In addition to these two signaling pathways, our analysis also revealed that the top WikiPathway was BDNF signaling for the top 100 genes. This agrees with the strong correlation of expression changes of BDNF knockout mice with human HD brain (Kuhn et al., 2007, Strand et al., 2007) and numerous studies showing that BDNF is neuroprotective in HD (Crane et al., 2014). All of these findings support the use of NSCs for studying HD in its developmental phases.

In conclusion, we report here that a HD NSC model provides evidence for early disruption of signaling pathways that are critical to establishing striatal lineage, and restoring these pathways either early or late in the disease process may provide disease-modifying therapies. Future work will focus on modulating these critical pathways in vivo to provide therapeutics treatments for HD.

EXPERIMENTAL PROCEDURES

Culture of iPSCs

All lines of iPSCs were grown on Matrigel (BD Biosciences) in mTeSR1 defined medium (STEMCELL). Optimal passaging occurred at 70%–80% confluency and was performed by treatment for 1 hr with 1 mg/ml collagenase. For RNA-seq sample preparation, comparison lines (HD iPSCs, C116 iPSCs) were grown and expanded in tandem for three passages before collection of total RNA. The isogenic lines (HD iPSCs and C116 iPSCs) were described in An et al. (2012) and Zhang et al. (2010) as well as further control lines. The non-isogenic HD iPSCs lines ND41656 (CAG57) and ND42222 (CAG109) were obtained from Coriell repository. The methods for differentiation to NSCs, RNA isolation, RNA-seq, qPCR, enrichment and network analysis, western blot of NSCs and zQ175 mice, caspase activity, and seahorse measurements are found in the Supplemental Experimental Procedures and previous publications (An et al., 2012; Zhang et al., 2010).

ACCESSION NUMBERS

The accession number for the RNA-seq data reported in this paper is GEO: GSE74201.

SUPPLEMENTAL INFORMATION

Supplemental Information includes Supplemental Experimental Procedures, three figures, and six tables and can be found with this article online at http://dx.doi.org/10.1016/j.stemcr.2015.11.005.

AUTHOR CONTRIBUTIONS

K.R., M.C.A., and N.Z. carried out experiments. K.R., M.C.A., N.Z., S.M., and L.M.E. designed experiments. K.R., M.C.A., N.Z, R.N.O., F.G., E.M.R., R.A., B.B., S.M., S.D.M., G.C., and L.M.E. performed analysis of the data sets. M.C.A., K.R., and L.M.E. wrote the paper. All authors edited and contributed to the manuscript preparation.

ACKNOWLEDGMENTS

The funding for this research was provided by the CHDI, Inc. (L.M.E.), NIH T32 AG000266 (L.M.E., R.N.O., and K.R.), and F32 NS080551 (R.N.O.) training grants. We acknowledge the support of the NINDS Informatics Center for Neurogenetics and Neurogenomics (P30 NS062691).

Received: May 4, 2015
Revised: November 2, 2015
Accepted: November 12, 2015
Published: December 8, 2015

REFERENCES

An, M.C., Zhang, N., Scott, G., Montoro, D., Wittkop, T., Mooney, S., Melov, S., and Ellerby, L.M. (2012). Genetic correction of Huntington's disease phenotypes in induced pluripotent stem cells. Cell Stem Cell *11*, 253–263.

Annes, J.P., Munger, J.S., and Rifkin, D.B. (2003). Making sense of latent TGFbeta activation. J. Cell Sci. *116*, 217–224.

Auerbach, R.K., Chen, B., and Butte, A.J. (2013). Relating genes to function: identifying enriched transcription factors using the ENCODE ChIP-Seq significance tool. Bioinformatics *29*, 1922–1924.

Bard, J., Wall, M.D., Lazari, O., Arjomand, J., and Munoz-Sanjuan, I. (2014). Advances in huntington disease drug discovery: novel approaches to model disease phenotypes. J. Biomol. Screen. *19*, 191–204.

Battaglia, G., Cannella, M., Riozzi, B., Orobello, S., Maat-Schieman, M.L., Aronica, E., Busceti, C.L., Ciarmiello, A., Alberti, S., Amico, E., et al. (2011). Early defect of transforming growth factor β1 formation in Huntington's disease. J. Cell. Mol. Med. *15*, 555–571.

Björkqvist, M., Wild, E.J., Thiele, J., Silvestroni, A., Andre, R., Lahiri, N., Raibon, E., Lee, R.V., Benn, C.L., Soulet, D., et al. (2008). A novel pathogenic pathway of immune activation detectable before clinical onset in Huntington's disease. J. Exp. Med. *205*, 1869–1877.

Bode, F.J., Stephan, M., Suhling, H., Pabst, R., Straub, R.H., Raber, K.A., Bonin, M., Nguyen, H.P., Riess, O., Bauer, A., et al. (2008). Sex differences in a transgenic rat model of Huntington's disease: decreased 17β-estradiol levels correlate with reduced numbers of DARPP32+ neurons in males. Hum. Mol. Genet. *17*, 2595–2609.

Camnasio, S., Delli Carri, A., Lombardo, A., Grad, I., Mariotti, C., Castucci, A., Rozell, B., Lo Riso, P., Castiglioni, V., Zuccato, C., et al. (2012). The first reported generation of several induced pluripotent stem cell lines from homozygous and heterozygous Huntington's disease patients demonstrates mutation related enhanced lysosomal activity. Neurobiol. Dis. *46*, 41–51.

Crane, A.T., Rossignol, J., and Dunbar, G.L. (2014). Use of genetically altered stem cells for the treatment of Huntington's disease. Brain Sci. *4*, 202–219.

Dennler, S., Goumans, M.J., and ten Dijke, P. (2002). Transforming growth factor beta signal transduction. J. Leukoc. Biol. *71*, 731–740.

Dias, J.M., Alekseenko, Z., Applequist, J.M., and Ericson, J. (2014). Tgfβ signaling regulates temporal neurogenesis and potency of neural stem cells in the CNS. Neuron *84*, 927–939.

Ehrlich, M.E. (2012). Huntington's disease and the striatal medium spiny neuron: cell-autonomous and non-cell-autonomous mechanisms of disease. Neurotherapeutics *9*, 270–284.

Evergren, E., Gad, H., Walther, K., Sundborger, A., Tomilin, N., and Shupliakov, O. (2007). Intersectin is a negative regulator of dynamin recruitment to the synaptic endocytic zone in the central synapse. J. Neurosci. *27*, 379–390.

Fogel, B.L., Cho, E., Wahnich, A., Gao, F., Becherel, O.J., Wang, X., Fike, F., Chen, L., Criscuolo, C., De Michele, G., et al. (2014). Mutation of senataxin alters disease-specific transcriptional networks in patients with ataxia with oculomotor apraxia type 2. Hum. Mol. Genet. *23*, 4758–4769.

Hamasaki, T., Goto, S., Nishikawa, S., and Ushio, Y. (2001). A role of netrin-1 in the formation of the subcortical structure striatum: repulsive action on the migration of late-born striatal neurons. J. Neurosci. *21*, 4272–4280.

Hayashi, T., Umemori, H., Mishina, M., and Yamamoto, T. (1999). The AMPA receptor interacts with and signals through the protein tyrosine kinase Lyn. Nature *397*, 72–76.

HD iPSC Consortium (2012). Induced pluripotent stem cells from patients with Huntington's disease show CAG-repeat-expansion-associated phenotypes. Cell Stem Cell *11*, 264–278.

Heiman, M., Schaefer, A., Gong, S., Peterson, J.D., Day, M., Ramsey, K.E., Suárez-Fariñas, M., Schwarz, C., Stephan, D.A., Surmeier, D.J., et al. (2008). A translational profiling approach for the molecular characterization of CNS cell types. Cell *135*, 738–748.

Hodges, A., Strand, A.D., Aragaki, A.K., Kuhn, A., Sengstag, T., Hughes, G., Elliston, L.A., Hartog, C., Goldstein, D.R., Thu, D., et al. (2006). Regional and cellular gene expression changes in human Huntington's disease brain. Hum. Mol. Genet. *15*, 965–977.

Hsiao, H.Y., Chiu, F.L., Chen, C.M., Wu, Y.R., Chen, H.M., Chen, Y.C., Kuo, H.C., and Chern, Y. (2014). Inhibition of soluble tumor necrosis factor is therapeutic in Huntington's disease. Hum. Mol. Genet. *23*, 4328–4344.

Kandasamy, M., Reilmann, R., Winkler, J., Bogdahn, U., and Aigner, L. (2011). Transforming growth factor-beta signaling in the neural stem cell niche: a therapeutic target for Huntington's disease. Neurol. Res. Int. *2011*, 124256.

Kaye, J.A., and Finkbeiner, S. (2013). Modeling Huntington's disease with induced pluripotent stem cells. Mol. Cell. Neurosci. *56*, 50–64.

Krupinski, J., Kumar, P., Kumar, S., and Kaluza, J. (1996). Increased expression of TGF-beta 1 in brain tissue after ischemic stroke in humans. Stroke *27*, 852–857.

Kuang, C., Xiao, Y., Yang, L., Chen, Q., Wang, Z., Conway, S.J., and Chen, Y. (2006). Intragenic deletion of Tgif causes defectsin brain development. Hum. Mol. Genet. *15*, 3508–3519.

Kuhn, A., Goldstein, D.R., Hodges, A., Strand, A.D., Sengstag, T., Kooperberg, C., Becanovic, K., Pouladi, M.A., Sathasivam, K., Cha, J.H., et al. (2007). Mutant huntingtin's effects on striatal gene expression in mice recapitulate changes observed in human Huntington's disease brain and do not differ with mutant huntingtin length or wild-type huntingtin dosage. Hum. Mol. Genet. *16*, 1845–1861.

Langfelder, P., and Horvath, S. (2008). WGCNA: an R package for weighted correlation network analysis. BMC Bioinformatics *9*, 559.

Langfelder, P., Mischel, P.S., and Horvath, S. (2013). When is hub gene selection better than standard meta-analysis? PLoS ONE *8*, e61505.

Lee, C.Y., Cantle, J.P., and Yang, X.W. (2013). Genetic manipulations of mutant huntingtin in mice: new insights into Huntington's disease pathogenesis. FEBS J. *280*, 4382–4394.

Lein, E.S., Hawrylycz, M.J., Ao, N., Ayres, M., Bensinger, A., Bernard, A., Boe, A.F., Boguski, M.S., Brockway, K.S., Byrnes, E.J., et al. (2007). Genome-wide atlas of gene expression in the adult mouse brain. Nature *445*, 168–176.

Liao, S.J., Gong, Q., Chen, X.R., Ye, L.X., Ding, Q., Zeng, J.S., and Yu, J. (2013). Netrin-1 rescues neuron loss by attenuating secondary apoptosis in ipsilateral thalamic nucleus following focal cerebral infarction in hypertensive rats. Neuroscience *231*, 225–232.

Lo Sardo, V., Zuccato, C., Gaudenzi, G., Vitali, B., Ramos, C., Tartari, M., Myre, M.A., Walker, J.A., Pistocchi, A., Conti, L., et al. (2012). An evolutionary recent neuroepithelial cell adhesion function of huntingtin implicates ADAM10-Ncadherin. Nat. Neurosci. *15*, 713–721.

Lobo, M.K., Karsten, S.L., Gray, M., Geschwind, D.H., and Yang, X.W. (2006). FACS-array profiling of striatal projection neuron subtypes in juvenile and adult mouse brains. Nat. Neurosci. *9*, 443–452.

Margueron, R., and Reinberg, D. (2011). The Polycomb complex PRC2 and its mark in life. Nature *469*, 343–349.

Miller, J.P., Yates, B.E., Al-Ramahi, I., Berman, A.E., Sanhueza, M., Kim, E., de Haro, M., DeGiacomo, F., Torcassi, C., Holcomb, J., et al. (2012). A genome-scale RNA-interference screen identifies RRAS signaling as a pathologic feature of Huntington's disease. PLoS Genet. *8*, e1003042.

Molero, A.E., Gokhan, S., Gonzalez, S., Feig, J.L., Alexandre, L.C., and Mehler, M.F. (2009). Impairment of developmental stem cell-mediated striatal neurogenesis and pluripotency genes in a knock-in model of Huntington's disease. Proc. Natl. Acad. Sci. USA *106*, 21900–21905.

Molina-Calavita, M., Barnat, M., Elias, S., Aparicio, E., Piel, M., and Humbert, S. (2014). Mutant huntingtin affects cortical progenitor cell division and development of the mouse neocortex. J. Neurosci. *34*, 10034–10040.

Onorati, M., Castiglioni, V., Biasci, D., Cesana, E., Menon, R., Vuono, R., Talpo, F., Goya, R.L., Lyons, P.A., Bulfamante, G.P., et al. (2014). Molecular and functional definition of the developing human striatum. Nat. Neurosci. *17*, 1804–1815.

Reis, S.A., Thompson, M.N., Lee, J.M., Fossale, E., Kim, H.H., Liao, J.K., Moskowitz, M.A., Shaw, S.Y., Dong, L., Haggarty, S.J., et al. (2011). Striatal neurons expressing full-length mutant huntingtin exhibit decreased N-cadherin and altered neuritogenesis. Hum. Mol. Genet. *20*, 2344–2355.

Sakuma, M., Tanaka, E., Taru, H., Tomita, S., Gandy, S., Nairn, A.C., Nakaya, T., Yamamoto, T., and Suzuki, T. (2009). Phosphorylation of the amino-terminal region of X11L regulates its interaction with APP. J. Neurochem. *109*, 465–475.

Selman, C., Lingard, S., Choudhury, A.I., Batterham, R.L., Claret, M., Clements, M., Ramadani, F., Okkenhaug, K., Schuster, E., Blanc, E., et al. (2008). Evidence for lifespan extension and delayed age-related biomarkers in insulin receptor substrate 1 null mice. FASEB J. *22*, 807–818.

Seong, I.S., Woda, J.M., Song, J.-J., Lloret, A., Abeyrathne, P.D., Woo, C.J., Gregory, G., Lee, J.-M., Wheeler, V.C., Walz, T., et al. (2010). Huntingtin facilitates polycomb repressive complex 2. Hum. Mol. Genet. *19*, 573–583.

Serra, H.G., Duvick, L., Zu, T., Carlson, K., Stevens, S., Jorgensen, N., Lysholm, A., Burright, E., Zoghbi, H.Y., Clark, H.B., et al. (2006). RORalpha-mediated Purkinje cell development determines disease severity in adult SCA1 mice. Cell *127*, 697–708.

Shi, L., Yue, J., You, Y., Yin, B., Gong, Y., Xu, C., Qiang, B., Yuan, J., Liu, Y., and Peng, X. (2006). Dok5 is substrate of TrkB and TrkC receptors and involved in neurotrophin induced MAPK activation. Cell. Signal. *18*, 1995–2003.

Southwell, A.L., Franciosi, S., Villanueva, E.B., Xie, Y., Winter, L.A., Veeraraghavan, J., Jonason, A., Felczak, B., Zhang, W., Kovalik, V., et al. (2015). Anti-semaphorin 4D immunotherapy ameliorates neuropathology and some cognitive impairment in the YAC128 mouse model of Huntington disease. Neurobiol. Dis. *76*, 46–56.

Strand, A.D., Baquet, Z.C., Aragaki, A.K., Holmans, P., Yang, L., Cleren, C., Beal, M.F., Jones, L., Kooperberg, C., Olson, J.M., and Jones, K.R. (2007). Expression profiling of Huntington's disease models suggests that brain-derived neurotrophic factor depletion plays a major role in striatal degeneration. J. Neurosci. *27*, 11758–11768.

The Huntington's Disease Collaborative Research Group. (1993). A novel gene containing a trinucleotide repeat that is expanded and unstable on Huntington's disease chromosomes. Cell *72*, 971–983.

Tourette, C., Farina, F., Vazquez-Manrique, R.P., Orfila, A.M., Voisin, J., Hernandez, S., Offner, N., Parker, J.A., Menet, S., Kim, J., et al. (2014). The Wnt receptor Ryk reduces neuronal and cell survival capacity by repressing FOXO activity during the early phases of mutant huntingtin pathogenicity. PLoS Biol. *12*, e1001895.

Vawter, M.P., Dillon-Carter, O., Tourtellotte, W.W., Carvey, P., and Freed, W.J. (1996). TGFbeta1 and TGFbeta2 concentrations are elevated in Parkinson's disease in ventricular cerebrospinal fluid. Exp. Neurol. *142*, 313–322.

Victorson, D., Carlozzi, N.E., Frank, S., Beaumont, J.L., Cheng, W., Gorin, B., Duh, M.S., Samuelson, D., Tulsky, D., Gutierrez, S., et al. (2014). Identifying motor, emotional-behavioral, and cognitive deficits that comprise the triad of HD symptoms from patient, caregiver, and provider perspectives. Tremor Other Hyperkinet. Mov. (N. Y.) *4*, 224.

Videnovic, A. (2013). Treatment of huntington disease. Curr. Treat. Options Neurol. *15*, 424–438.

Zetterberg, H., Andreasen, N., and Blennow, K. (2004). Increased cerebrospinal fluid levels of transforming growth factor-beta1 in Alzheimer's disease. Neurosci. Lett. *367*, 194–196.

Zhang, N., An, M.C., Montoro, D., and Ellerby, L.M. (2010). Characterization of human Huntington's disease cell model from induced pluripotent stem cells. PLoS Curr. *2*, RRN1193.

Stem Cell Reports, Volume *5*

Supplemental Information

Genomic Analysis Reveals Disruption of Striatal Neuronal Development and Therapeutic Targets in Human Huntington's Disease Neural Stem Cell

Karen L. Ring, Mahru C. An, Ningzhe Zhang, Robert N. O'Brien, Eliana Marisa Ramos, Fuying Gao, Robert Atwood, Barbara J. Bailus, Simon Melov, Sean D. Mooney, Giovanni Coppola, and Lisa M. Ellerby

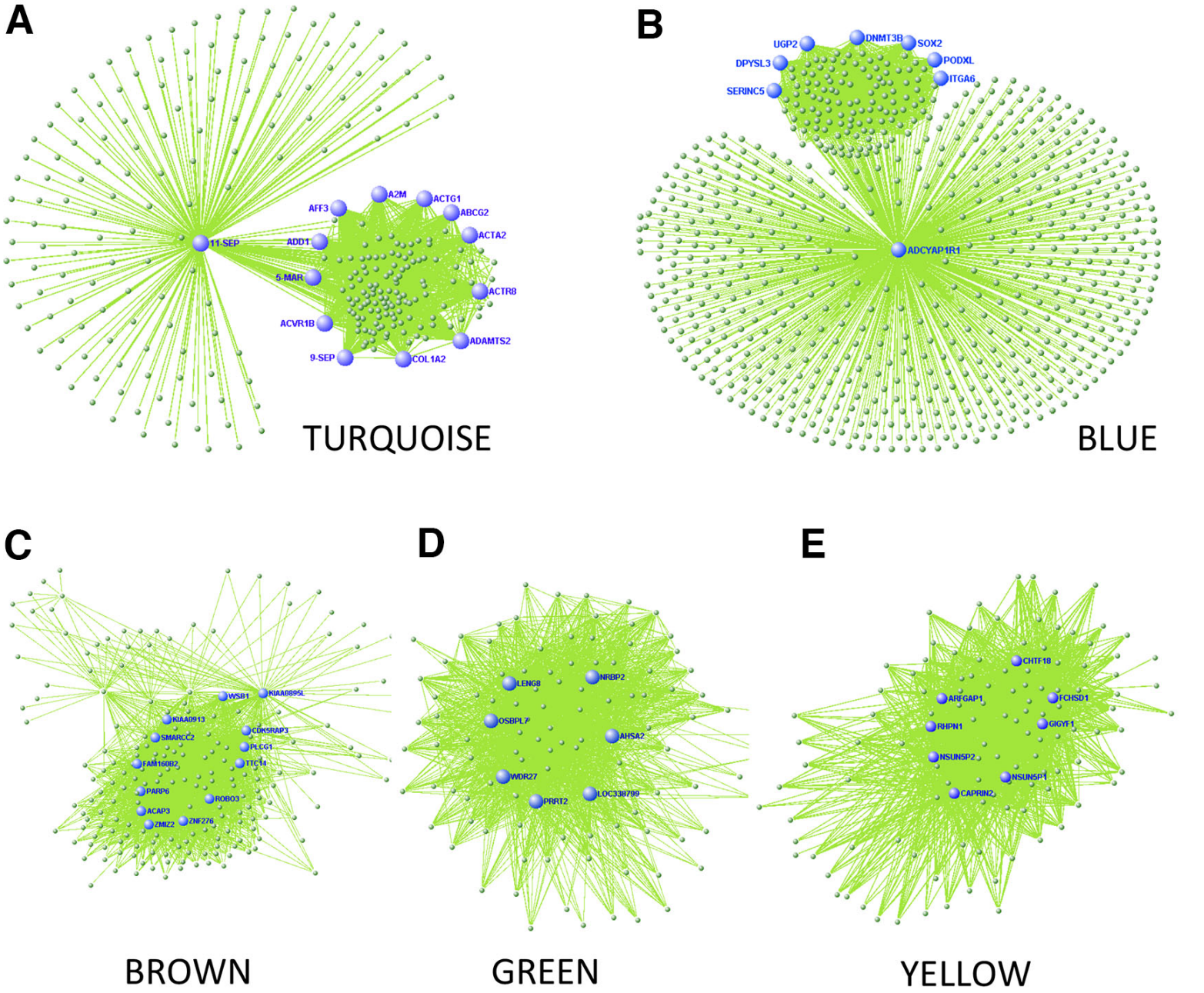
A
11-SEP
AFF3
A2M
ACTG1
ABCG2
ADD1
ACTA2
5-MAR
ACTR8
ACVR1B
ADAMTS2
9-SEP
COL1A2
TURQUOISE
B
UGP2
DNMT3B
SOX2
DPYSL3
PODXL
ITGA6
SERINC5
ADCYAP1R1
BLUE
C
WSB1
KIAA0895L
KIAA0913
SMARCC2
CDK5RAP3
PLCG1
FAM160B2
TTC14
PARP6
ROBO3
ACAP3
ZMIZ2
ZNF276
BROWN
D
LENG8
NRBP2
OSBPL7
AHSA2
WDR27
PRRT2
LOC338799
GREEN
E
CHTF18
ARFGAP1
FCHSD1
RHPN1
GIGYF1
NSUN5P2
NSUN5P1
CAPRIN2
YELLOW

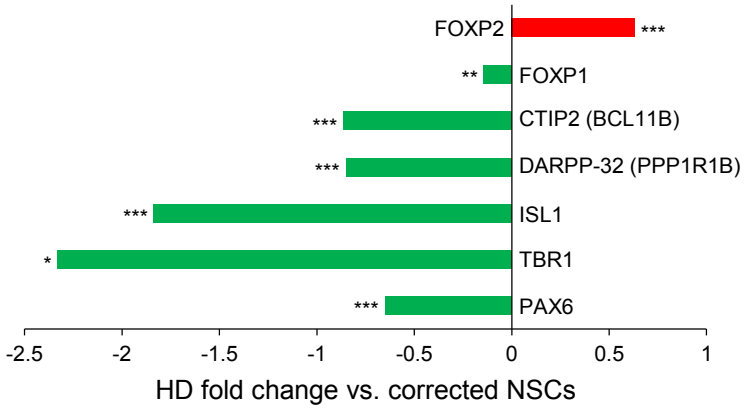
FOXP2
***
**
FOXP1
***
CTIP2 (BCL11B)
***
DARPP-32 (PPP1R1B)
***
ISL1
*
TBR1
***
PAX6
-2.5
-2
-1.5
-1
-0.5
0
0.5
1
HD fold change vs. corrected NSCs

A

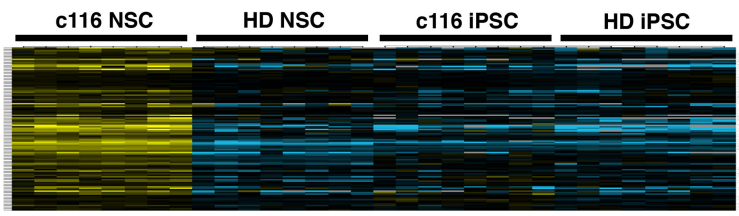

B

Term	P-value	Z-score	Combined Score	Genes
dorsal_striatum	0.047	-1.896	5.788	PPP1R1B;LRRTM1;TAC1;SCN4B;MCHR1
mIMCD-3	0.036	-1.697	5.647	ABCC4;HOXB9;CLCF1;CDH6
liver	0.037	-1.575	5.196	C2;LETMD1;NNMT;IGFBP7;TLCD2;HAAO;INSIG1;BCAS3;RETSAT
nih_3T3	0.086	-1.443	3.533	BDNF;TBX18;CRABP1
macrophage_bone_marrow_24h_LPS	0.191	-1.715	2.836	BCL2L2;GNGT2;PTK2B;TSPO
osteoclasts	0.077	-1.028	2.639	KCNJ2;DENND1B
mammary_gland__lact	0.070	-0.898	2.391	STAT5A;G0S2
uterus	0.116	-0.958	2.064	PADI1;COL6A3;TGM2
heart	0.206	-1.294	2.047	SLC8A1;EXT2;RBM20;MYL3
nucleus_accumbens	0.209	-1.276	1.998	PPP1R1B;MCHR1;TAC1

C

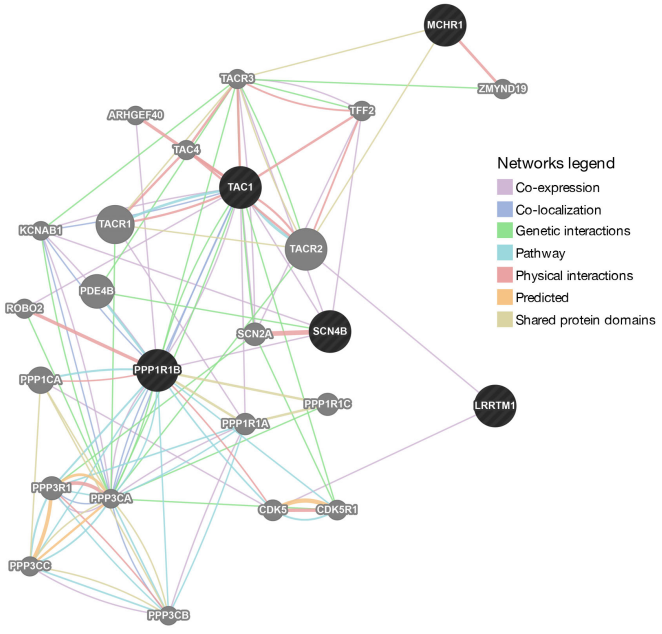

SUPPLEMENTAL FIGURE LEGENDS

Fig. S1. Hub connectivity of module genes, visualized for the five remaining modules. (**A-E**) Network plot depicting the top connections for each module. Most highly connected module members (or hub genes) are shown for each group.

Fig. S2. Expression levels of these critical striatal genes are altered in neural stem cells from HD NSCs. Colored bars indicate RNA expression level fold-change in $\log_2$ scale of human HD vs. corrected NSCs for genes prominently expressed during striatal development. All genes shown were statistically significant when adjusted for FDR, with *$p < 0.05$, **$p < 0.005$, ***$p < 0.0005$.

Fig. S3. Hierarchical clustering approach reveals down regulated genes in HD NSCs linked to BDNF signaling. (A) Expression trait profiles across all 32 samples for module gene members. (**B**) Gene enrichment of module gene members, top hit is dorsal striatum. (**C**) Visualization of networks associated with top term gene members using the Genemania tool.

Table S4. Go Annotation of WGCNA Modules using DAVID Analysis

Module	Select Hub Genes	Top Biological Processes Associated with Module
Blue	ADCYAP1R1, SERINC5, DPYSL3, UGP2, DNMT3B, SOX2, PODXL, ITGA6	Translation, metabolic process, proteasomal protein catabolic process, proteasomal ubiquitin-dependent protein catabolic process, tRNA metabolic process, ribosome biogenesis, cellular macromolecule catabolic process
Turquoise	SEPT11, AFF3, A2M, ACTG1, ABCG2, ACTA2, ACTR8, ADAMTS2, COL1A2, SEPT9, ACVR1B, MARCH5	Regulation of transcription, transcription, regulation of RNA metabolic process, regulation of transcription, DNA-dependent, chromatin modification, chromosome organization, chromatin organization, cell cycle, response to DNA damage stimulus
Black	HSPB8, DOK5, SH3BGRL2, VGLL3, LYN, GRIP1, FAM131B, EFEMP1	None significant
Red	SEMA3D, IRS1, CDH2, APBB2	Neuron projection morphogenesis, cell projection organization, cell motion, cell projection morphogenesis, cell part morphogenesis, neuron projection development, neuron differentiation, cellular component morphogenesis, neuron development, axonogenesis
Yellow	CHTF18, FCHSD1, GIGYF1, NSUN5P1, NSUN5P2, CAPRIN2, RHPN1, ARFGAP1	Chromatin modification, DNA repair, DNA metabolic process, cellular response to stress, response to DNA damage stimulus, DNA recombination, chromatin organization, chromosome organization, striated muscle cell development, muscle cell development
Brown	WSB1, KIAA0895L, CDK5RAP3, PLCG1, TTC14, ROBO3, ZNF276, ZMIZ2, ACAP3, PARP6, FAM160B2, SMARCC2, KIAA0913	Negative regulation of gene expression, negative regulation of nucleobase, nucleoside, nucleotide and nucleic acid metabolic process, negative regulation of nitrogen compound metabolic process, negative regulation of macromolecule biosynthetic process, negative regulation of cellular biosynthetic process, negative regulation of transcription, DNA dependent, negative regulation of transcription
Green	LENG8, NRBP2, AHSA2, LOC338799, PRRT2, WDR27, OSBPL7, LENG8	Regulation of protein kinase activity, regulation of kinase activity, regulation of transferase activity

SUPPLEMENTAL PROCEDURES

Differentiation and Culture of NSCs

NSCs were generated with STEMdiff Neural Induction Medium from Stemcell Technologies according to manufacturer's manual. Briefly 70-80% confluent iPSCs were detached and dissociated to single cells by incubation in Accutase (Sigma) at 37^{o}C for 5-10 min. 4 X 10^{6} cells were seeded in one well of a AggreWell 800 plate (Stemcell Technologies) in STEMdiff Neural Induction Medium supplemented with Y27632 ROCK inhibitor (10 μM, Calbiochem). After 5 days of culture in AggreWell 800 plate, neural aggregates formed in the grids of the well were transferred and attached to poly-L-ornithine/laminin coated culture dish. After 7 more days of culture in STEMdiff Neural Induction Medium, rosettes were harvested by incubation in STEMdiff Neural Rosette Selection Reagent at 37^{o}C for 1h followed by washing in DMEM/F12 medium (Life Technologies). Rosettes were triturated with a P1000 tip for 3 times and seeded in poly-L-ornithine/laminin coated culture dish in neural proliferation medium (Neurobasal medium supplemented with 1X B27, 2mM L-Glutamine, 25 ng/ml bFGF, 10 ng/ml LIF, 100 U/ml penicillin and 100 μg/ml streptomycin). NSCs were expanded on Matrigel (Corning) coated dishes and passaged with Accutase. NSCs were over 98% nestin positive (An et al. 2012). After seven passages, NSC samples were harvested in 60 mm dishes with N = 8 for RNA-Seq.

RNA Isolation

Total RNA was purified from iPSCs, NSCs or neurons using RNeasy Mini kit (Qiagen). For RNA-Seq samples, an additional 350 μl RLT/β-mercaptoethanol solution were added to each tube, followed by vortexing and centrifugation to lyse the cells. A Qiacube instrument was then used to extract the RNA using the RNase Micro protocol. The samples were eluted in 25 μl PCR grade H_20. Sample OD was obtained by nanodrop for QC and then diluted to 4ng/40 μl.

RNA-Seq

Subsequent RNA-Seq by IIlumina library preparation on a Illumina Hiseq 2000 sequencer was performed by the core genomics facility at the University of Minnesota. 32 libraries were prepared, size selected (average insert size of ~200bp) and barcoded using TruSeq RNA Library preparation kits and sequenced using a 50bp paired-end protocol, yielding on average 20 million reads per library. Average quality scores for all libraries was above Q30. The RNAseq data set is under accession number GSE74201.

Unique reads were mapped to the genome using Bowtie or ClCBio, and differential expression analysis was performed using edgeR (Robinson et al., 2010). False discovery rate (FDR) was set at 0.05.

For WCGNA analysis, reads were aligned to the human hg19 reference genome using the STAR spliced read aligner (Dobin et al., 2013) with default parameters. Total counts of read-fragments aligned to candidate gene regions were obtained using the HTSeq program (Anders et al., 2015) and used as a basis for quantification of gene expression. Differential gene expression analysis between sample groups of interest was

performed using edgeR (Robinson et al., 2010) and the FDR set at 0.05. Normalized expression levels were used to perform WCGNA using the WGCNA package (Langfelder and Horvath, 2008) as previously described (Gu et al., 2015). Briefly, a topological overlap matrix was generated, and genes were clustered based on topological overlap, a measure of network connectivity. Using dynamic tree cutting, groups of coexpressed genes, or modules, were identified.

Enrichment and Networking Analysis

Relevant gene lists or module members were inputted into Enrichr tools (Mount Sinai School of Medicine) (Chen et al., 2013). Enrichment terms are scored by p-value, z-score, and combined score, and shown in figures sorted by combined score. Gene members of relevant terms were further investigated using Genemania (University of Toronto). In a recent paper by Onorati et al. 2014, members of the M25 WGCNA module were identified as being highly expressed in the human striatum (Onorati et al., 2014). We compared the gene symbols found in our black module with those found in the M25 module using the hypergeometric statistical test.

A permutation test was performed to assess over-representation of module genes in HD relevant gene sets curated from the literature (GeneSet lists), namely, striatum-specific mouse genes (top 100) identified from the Allen Brain Atlas (Lein et al. 2007), human caudate (Strand et al. 2007a) and developing human striatum (Onorati et al. 2014) enriched gene sets, medium spiny neuron enriched gene sets from three publications (Hodges et al. 2006, Heiman et al. 2008 and Lobo et al. 2006), and

deregulated genes in a BDNF knockout mouse model (Strand et al. 2007b). For the 2 HD-relevant modules (black and red), overlap with each GeneSet list was determined, as well as the overlap of randomly generated gene lists from the background (with the same number of genes in the module) with each GeneSet list (10,000 permutations). Z-score was calculated as the number of standard deviations our observed value was above the mean of the observed values within the empirical null distribution. The background was set to the total list of genes expressed in our data set (n=13,952 genes).

Additionally, the ENCODE ChIP-Seq significance tool (Auerbach et al. 2013) was used to identify enriched transcription factors in the 2 HD-relevant modules (black and red). Briefly, this tool determines the number of genes in each gene module list with at least one TF peak in the selected window and then calculates enrichment scores (Q-value) using one-tailed hypergeometric test followed by multiple hypothesis correction (FDR method). For our queries we used an upstream and downstream analysis window of 1,000bp from the transcription start site. The background was set to the total list of genes expressed in our data set (n=13,952 genes).

Hierarchical Clustering Analysis

In order to complement our WGCNA analysis, we performed hierarchical clustering using an independent analysis method. Genes displaying significant changes were log2 transformed, while genes with data missing in 8 or more samples (25% of total samples) were excluded. The resulting data (7290 genes, 32 arrays) were clustered by centroid linkage hierarchical clustering using Cluster 3.0 (de Hoon et al. 2004; Eisen et al. 1998).

Modules were analyzed by Genemania (Mostafavi et al., 2008).

RT-qPCR

RNA (1µg) was converted to cDNA by using the Message Sensor RT kit (Life Technologies). Real time quantitative PCR (qPCR) was performed with Universal Probe Library dye (UPL from Roche) on the LightCycler 480 system (Roche). For quantification the threshold cycle Cp of each amplification was determined by the 2nd derivative analysis provided by the LightCycler 480 software and the $2^{-\Delta\Delta Cp}$ method was used to determine the relative expression level of each gene normalized against the house-keeping gene β-actin (ActB). The primers for DARPP-32 (PPP1R1B) were forward: 5'-CACACCACCTTCGCTGAAA-3', reverse: 5'-GAAGCTCCCCCAGCTCAT-3'; netrin-1 (NTN1), forward 5'-CCCTGCATAAAGATCCCTGT-3', reverse 5'-TTGCAGTAGGAATCGCAGTC-3'; TGFβ1 (TGFB1), forward 5'-AGTGGTTGAGCCGTGGAG-3', reverse 5'-TGCAGTGTGTTATCCCTGCT-3'. The primers for β-actin (ACTB) were forward: 5'-CCAACCGCGAGAAGATG-3', reverse: 5'-CCAGAGGCGTACAGGGATAG-3'.

Western Blot Analysis

HD or corrected NSCs were cultured to 90-100% confluency. Media was removed and cells were lysed by sonication in an M-PER (Thermo-Scientific) solution containing protease inhibitors (Complete mini tablet per 10 ml buffer; Roche), phosphatase inhibitors (100 µl/10 ml buffer; Calbiochem # III and IV), and DNase (New England Biolabs; 100 units/10 ml buffer;). For TGF-β western blotting, 20 µg of each protein

sample was loaded onto a 12% Bis-Tris gel (Invitrogen) in MOPS buffer (Life Technologies) and run at 200 volts for 50-60 min. Protein bands were transferred onto a 0.45 PVDF membrane (Millipore) that was previously activated by soaking in 100% methanol. Transfer buffer was supplemented with 10% methanol, and the transfer was carried out at 4°C for 1h at 350 milliAmp. Following transfer, membranes were blocked in 5% milk for 1h and then probed over night with rabbit anti-TGF-β (Abcam, ab66043) at 1:100-1:500. The following day, blots were washed and then probed with anti-rabbit HRP secondary (GE Healthcare) for 1h at 1:4000. For pSMAD2 and SMAD2 western blotting, protein samples were run on a 4-12% Bis-Tris gel at 200 volts for 1h. Protein was transferred to nitrocellulose membranes (Whatman) and blots were blocked and probed in 5% milk. Anti-pSMAD2 and SMAD2 were used at 1:200-1:500 (Cell Signaling Technologies, #3101, #5339). Tubulin antibody was used at 1:2000 (Sigma, T6199) and rabbit β-actin at 1:500 (Cell Signaling, #4968S).

Caspase-3/7 Assay

HD and corrected NSCs were passaged and grown to confluency in neural proliferation medium (NPM) supplemented with 25 ng/ml FGF-2. 96 well plates were coated with matrigel for 1h at 37^{o}C before seeding 3x10^{4} NSCs per well in NPM with 25ng/ml FGF-2. 24h post seeding, media was removed and cells were washed once with PBS. Cells were then treated for 48h with complete medium (NPM, FGF-2), basic medium (neurobasal media only), or basic medium with TGF-β1 or TGF-β2 at 10 ng/ml (Peprotech). After 48h,

caspase-3/7 activity assays were conducted using the APO3 HTS kit and the Fusion Alpha Universal Microplate Analyzer, as previously described (Zhang et al., 2010).

Respirometry Analysis

The respirometry analysis of NSCs was carried out using an XF24 extracellular flux analyzer (Seahorse Bioscience). Both HD NSCs and corrected C116 NSCs were seeded in an XF24 cell culture microplate with standard culture conditions. 90% confluent cells were pre-treated with 100ng/ml netrin-1 or 50ng/ml TGF-β1 for 24h in normal full medium followed by 12h treatment in basic medium (Neurobasal medium only) with same doses of netrin-1 or TGF-β1. Right before respirometry analysis, cells were washed three times with "Seahorse buffer" (120mM NaCl, 3.5mM KCl, 1.3mM $CaCl_2$, 0.4mM KH_2PO_4, 20mM TES, 1.2mM Na_2SO_4, 2mM $MgCl_2$, 15mM glucose, 15mM sodium pyruvate, pH7.4) and left in "Seahorse buffer" at 37^{o}C. The plate was loaded into the XF24 analyzer for a program with 13 cycles of 1min mix, 2min wait and 3min measurement. 2μg/ml oligomycin was added into cells after the 4th cycle. 1uM FCCP was added after the 7th cycle. 2uM rotenone and 1uM antimycin-A were added after the 10th cycle. The oxygen consumption was shown as pMole O_2/min after normalization against protein concentration measured by BCA protein assay kit.

zQ175 Knockin Mice

The mouse strain was housed at the Animal Facility of the Buck Institute for Research on Aging. We are an AAALAC international accredited institution (Unit #001070) and all

procedures were approved by the Institutional Animal and Care and Use Committee (A4213-01). Wild type and zQ175 mouse brains were dissected into the indicated regions. Samples were flash frozen on dry ice and stored immediately at -80^{o}C until tissue homogenization. Homogenization buffer consisted of 10ml TPER (Thermo Scientific, cat#78510) supplemented with protease inhibitors (Roche, 1 tablet/10 ml, Complete Mini, EDTA-free, cat#11836153001), 1µl DNAse (Invitrogen, cat#18047-019, 250U/µl), 1.2 mM $MgCl_2$ (Fluka, cat# 63543), 1 µM Epoxomycin (Sigma, cat#D4321-1MG), 100 µl phosphatase inhibitor cocktail II (Calbiochem PPI II, cat#524625). HDAC activity was inhibited by a cocktail of HDAC inhibitors composed of 50 µM TSA (Sigma, cat#T8552-5MG), 30 mM Nicotinamide (Sigma, cat#N0636-100G) and 30 µM sodium butyrate (Sigma, cat#19364) added to the resuspension buffer. A 2ml dounce homogenizer was used for cell lysis on ice (2 x 60 pumps with a 30 s interval). Samples were stored at -80^{o}C prior to sonication. Tissue lysates were sonicated with continuous 40 mA pulses for 5s x5 on ice. Sonicated samples were centrifuged at 14,000 g and 4^{o}C on a 5417 Eppendorf centrifuge for 20 min. Supernatant was collected for western blot analysis as described above.

Statistical Comparisions

Statistical significance between the different groups was performed by 2-way ANOVA Graphpad Prism software (La Jolla, CA) and comparisons were significant when * $p < 0.05$, ** $p< 0.005$, *** $p< 0.001$ and **** $p< 0.0005$. Data is presented as mean and SD. Biological replicates (BR) refers to the sample grown in separate culture plates under

the similar conditions. Statistical analysis was performed on at least 3 independent replicates or animal samples.

REFERENCES

An, M.C., Zhang, N., Scott, G., Montoro, D., Wittkop, T., Mooney, S., Melov, S., and Ellerby, L.M. (2012). Genetic correction of Huntington's disease phenotypes in induced pluripotent stem cells. Cell Stem Cell *11*, 253-263.

Anders, S., Pyl, P.T., and Huber, W. (2015). HTSeq--a Python framework to work with high-throughput sequencing data. Bioinformatics *31*, 166-169.

Auerbach RK, Chen B, Butte AJ (2013). Relating genes to function: identifying enriched transcription factors using the ENCODE ChIP-Seq significance tool. Bioinformatics *29*, 1922-1924.

Chen, E.Y., Tan, C.M., Kou, Y., Duan, Q., Wang, Z., Meirelles, G.V., Clark, N.R., and Ma'ayan, A. (2013). Enrichr: interactive and collaborative HTML5 gene list enrichment analysis tool. BMC bioinformatics *14*, 128.

de Hoon, M.J., Imoto, S., Nolan, J., and Miyano, S. (2004). Open source clustering software. Bioinformatics *20*, 1453-1454.

Dobin, A., Davis, C.A., Schlesinger, F., Drenkow, J., Zaleski, C., Jha, S., Batut, P., Chaisson, M., and Gingeras, T.R. (2013). STAR: ultrafast universal RNA-seq aligner. Bioinformatics *29*, 15-21.

Eisen, M.B., Spellman, P.T., Brown, P.O., and Botstein, D. (1998). Cluster analysis and display of genome-wide expression patterns. PNAS *95*, 14863-14868.

Gu, X., Cantle, J.P., Greiner, E.R., Lee, C.Y., Barth, A.M., Gao, F., Park, C.S., Zhang, Z., Sandoval-Miller, S., Zhang, R.L*., et al.* (2015). N17 Modifies Mutant Huntingtin Nuclear Pathogenesis and Severity of Disease in HD BAC Transgenic Mice. Neuron *85*, 726-741.

Heiman M, Schaefer A, Gong S, Peterson JD, Day M, Ramsey KE, Suárez-Fariñas M, Schwarz C, Stephan DA, Surmeier DJ et al. (2008). A translational profiling approach for the molecular characterization of CNS cell types. Cell *135*,738-748.

Hodges A, Strand AD, Aragaki AK, Kuhn A, Sengstag T, Hughes G, Elliston LA, Hartog C, Goldstein DR, Thu D et al. (2006) Regional and cellular gene expression changes in human Huntington's disease brain. Hum Mol Genet *15*, 965-977.

Langfelder, P., and Horvath, S. (2008). WGCNA: an R package for weighted correlation network analysis. BMC Bioinformatics *9*, 559.

Lein ES, Hawrylycz MJ, Ao N, Ayres M, Bensinger A, Bernard A, Boe AF, Boguski MS, Brockway KS, Byrnes EJ et al. (2007). Genome-wide atlas of gene expression in the adult mouse brain. Nature *445*, 168-176.

Lobo MK, Karsten SL, Gray M, Geschwind DH, Yang XW (2006). FACS-array profiling of striatal projection neuron subtypes in juvenile and adult mouse brains. Nat Neurosci *9*, 443-452.

Mostafavi, S., Ray, D., Warde-Farley, D., Grouios, C., and Morris, Q. (2008). GeneMANIA: a real-time multiple association network integration algorithm for predicting gene function. Genome biology *9 Suppl 1*, S4.

Onorati, M., Castiglioni, V., Biasci, D., Cesana, E., Menon, R., Vuono, R., Talpo, F., Goya, R.L., Lyons, P.A., Bulfamante, G.P.*, et al.* (2014). Molecular and functional definition of the developing human striatum. Nat Neurosci *17*, 1804-1815.

Robinson, M.D., McCarthy, D.J., and Smyth, G.K. (2010). edgeR: a Bioconductor package for differential expression analysis of digital gene expression data. Bioinformatics *26*, 139-140.

Strand AD, Aragaki AK, Baquet ZC, Hodges A, Cunningham P, Holmans P, Jones KR, Jones L, Kooperberg C, Olson JM (2007a). Conservation of regional gene expression in mouse and human brain. PLoS Gen 3(4):e59.

Strand, A.D., Baquet, Z.C., Aragaki, A.K., Holmans, P., Yang, L., Cleren, C., Beal, M.F., Jones, L., Kooperberg, C., Olson, J.M.*, et al.* (2007b). Expression profiling of Huntington's disease models suggests that brain-derived neurotrophic factor depletion plays a major role in striatal degeneration. J Neurosci *27*, 11758-11768.

Zhang, N., An, M.C., Montoro, D., and Ellerby, L.M. (2010). Characterization of Human Huntington's Disease Cell Model from Induced Pluripotent Stem Cells. PLoS Curr *2*, RRN1193.